The dynein cortical anchor Num1 activates dynein motility by relieving Pac1/LIS1-mediated inhibition

Lindsay G. Lammers and Steven M. Markus

Department of Biochemistry and Molecular Biology, Colorado State University, Fort Collins, CO 80523

Cortically anchored dynein orients the spindle through interactions with astral microtubules. In budding yeast, dynein is offloaded to Num1 receptors from microtubule plus ends. Rather than walking toward minus ends, dynein remains associated with plus ends due in part to its association with Pac1/LIS1, an inhibitor of dynein motility. The mechanism by which dynein is switched from "off" at the plus ends to "on" at the cell cortex remains unknown. Here, we show that overexpression of the coiled-coil domain of Num1 specifically depletes dynein–dynactin–Pac1/LIS1 complexes from microtubule plus ends and reduces dynein-Pac1/LIS1 colocalization. Depletion of dynein from plus ends requires its microtubule-binding domain, suggesting that motility is required. An enhanced Pac1/LIS1 affinity mutant of dynein or overexpression of Pac1/LIS1 rescues dynein plus end depletion. Live-cell imaging reveals minus end–directed dynein–dynactin motility along microtubules upon overexpression of the coiled-coil domain of Num1, an event that is not observed in wild-type cells. Our findings indicate that dynein activity is directly switched "on" by Num1, which induces Pac1/LIS1 removal.

Introduction

Cytoplasmic dynein is a 1.2-MD multisubunit motor complex that powers movement of various cargoes toward the minus ends of microtubules. This ancient and highly conserved ATPase organizes the intracellular environment throughout the cell cycle; however, its myriad roles become especially apparent during mitosis when it functions in various aspects of spindle morphogenesis and positioning (Rusan et al., 2002; Goshima et al., 2005; Yang et al., 2007; Ferenz et al., 2009; Siller and Doe, 2009). For instance, cortically anchored dynein motors position the spindle at the future site of cytokinesis (Eshel et al., 1993; Li et al., 1993; Carminati and Stearns, 1997), a process that is particularly important during asymmetric cell divisions, when spindle position dictates the plane of cell division, and thus cell fate determination (Pease and Tirnauer, 2011; Williams et al., 2011). The means by which dynein is delivered to the cell cortex and subsequently activated to pull on astral microtubules emanating from spindle poles to move the spindle are unclear.

Recent studies in budding and fission yeast have revealed two distinct mechanisms by which dynein can be targeted to the cell cortex, its site of action in both organisms (Markus and Lee, 2011; Ananthanarayanan et al., 2013). During the meiotic prophase in fission yeast, studies suggest that dynein first binds along astral microtubules that are in close proximity to the cell cortex (Ananthanarayanan et al., 2013). Rather than walking toward the minus end of these microtubules, dynein undergoes one-dimensional diffusion until it encounters Mcp5, its cortical anchor. Once bound to Mcp5, dynein mo-

tors switch from diffusive to directed motion and consequently move the spindle appropriately. Thus, in addition to anchoring dynein at the cortex, Mcp5 appears to activate dynein motility by an unknown mechanism.

A similar but somewhat distinct scenario takes place in budding yeast, in which dynein is first targeted to the plus ends of astral microtubules before being offloaded to cortical Num1 (Mcp5 homologue) receptor sites, where it functions to move the mitotic spindle toward the daughter cell (Adames and Cooper, 2000; Lee et al., 2005; Markus and Lee, 2011). It is unknown if dynein motility is activated subsequent to offloading; however, several lines of evidence suggest that its activity is switched from being off at plus ends to being on at the cell cortex. For instance, in spite of its minus end–directed motility, dynein is transported to, and remains associated with, the plus ends of dynamic microtubules (Lee et al., 2003; Carvalho et al., 2004). Plus end targeting requires the dynein motor domain, the +TIP (plus end–tracking protein) Bik1 (CLIP-170 homologue), and the dynein-associated factor Pac1 (homologue of human LIS1; Lee et al., 2003; Sheeman et al., 2003; Markus et al., 2009). Recent studies suggest that Pac1 plays two distinct and important roles in targeting dynein to plus ends. First, Pac1 mediates the interaction between dynein and plus end–bound Bik1 (Sheeman et al., 2003; Roberts et al., 2014). Second, by inhibiting dynein motility (Markus and Lee, 2011; Huang et al., 2012), and/or by prolonging its microtubule attachment (Yamada et al., 2008;

Correspondence to Steven M. Markus: steven.markus@colostate.edu

Abbreviations used in this paper: MTBD, microtubule-binding domain; PH, pleckstrin homology; SPB, spindle pole body.

Supplemental Material can be found at:
http://jcb.rupress.org/content/suppl/2015/10/15/jcb.201506119.DC1.html

McKenney et al., 2010; Huang et al., 2012), Pac1 holds dynein at plus ends by keeping dynein in a nonmotile, or "off" state. Thus, plus end–associated dynein may be poised to walk toward the minus ends of microtubules but is prevented from doing so by Pac1. However, upon offloading to cortical Num1 receptor sites, dynein is active, as apparent by its capacity to pull on astral microtubules and consequently move the spindle. Thus, in budding yeast, as in fission yeast, dynein may undergo a switch in its activity upon attachment to its cortical receptor. However, evidence for such a switch is lacking.

Although factors have been identified that can inhibit dynein motility (e.g., MAP4, She1, and Pac1; Markus and Lee, 2011; Samora et al., 2011; Huang et al., 2012; Markus et al., 2012), it remains unclear whether dynein from organisms other than fission yeast need to be switched on to perform their cellular functions or whether they are constitutively active. Recent studies indicated that purified metazoan dynein is functional for motility in ensemble assays (e.g., microtubule gliding) but requires a stable interaction with the dynactin complex for single-molecule processivity (McKenney et al., 2014; Schlager et al., 2014). Stabilization of the dynein–dynactin interaction by various coiled-coil–containing adaptor proteins (e.g., BicD2, Spindly, Hook3, and Rab11-Fip3) is sufficient to significantly enhance dynein processivity, and thereby "activate" dynein motility. This is in contrast to budding yeast dynein, which is processive in the absence of dynactin or other adaptors or regulators (Reck-Peterson et al., 2006). It is unclear whether such a mechanism generally governs dynein regulation within a cell, given that certain functions of dynein in animal cells, such as centrosome anchoring, pole focusing, and spindle length regulation, have been shown to occur independently of several such adaptors (Raaijmakers et al., 2013). It is also unclear whether dynactin-mediated processivity enhancement is the means by which cortical dynein activity is promoted. Interestingly, plus end association of dynein in higher eukaryotes, which occurs in a dynactin-dependent manner, does not require such adaptor proteins (Splinter et al., 2012; Duellberg et al., 2014). Given the lack of minus end–directed motility of these plus end–associated dynein motors, an interaction between dynein and dynactin is not necessarily sufficient to active dynein motility.

Using budding yeast, we aimed to test the hypothesis that binding of dynein–dynactin to its cortical receptor provides the switch that activates cortical dynein activity. Dynein pathway function is best understood in this genetically tractable organism, in which many of the regulatory components and accessory chains, which are each encoded by only one gene, are highly conserved. We found that overexpression of the dynein–dynactin–interacting coiled-coil domain of Num1 ($Num1_{CC}$) is sufficient to activate dynein motility, causing a depletion of dynein–dynactin from microtubule plus ends, their accumulation at minus ends, and their apparent minus end–directed motility along astral microtubules. Our data reveal that the mechanism for this activation is likely a $Num1_{CC}$-mediated release of Pac1, a potent dynein inhibitor, from the dynein motor domain.

Results

Overexpression of $Num1_{CC}$ depletes dynein–dynactin from microtubule plus ends

A recent study revealed that the N-terminal coiled-coil domain of Num1—the dynein cortical receptor—directly interacts with dynein–dynactin complexes (Tang et al., 2012). If this region of Num1 ($Num1_{CC}$; Fig. 1 A) is sufficient to activate dynein motility, we reasoned that its overexpression would result in (a) the depletion of dynein and dynactin from microtubule plus ends, and (b) an accumulation of dynein–dynactin at spindle pole bodies (SPBs), where microtubule minus ends are anchored (Fig. 1 B). We found this latter phenomenon to be an inherent property of dynein motility, because single-molecule motility experiments demonstrated that upon reaching the end of a microtubule, dynein pauses for several seconds before detaching, much longer than the dwell time of ∼0.1 s per step (Fig. S1 and Video 1). To test our hypothesis, we engineered yeast cells such that the galactose-inducible *GAL1* promoter (*GAL1p*) was immediately upstream of a truncated *num1_CC* allele (Fig. 1 C). Because $Num1_{CC}$ is expressed from the native *NUM1* locus, these cells do not possess a full-length Num1. Consequently, dynein and dynactin are excluded from the cell cortex and are unable to properly orient the spindle in these cells.

In the absence of $Num1_{CC}$ induction (by growth in glucose-containing media), we observed fluorescent foci of functional Dyn1- (dynein heavy chain) and Jnm1-3mCherry (p50 subunit of dynactin) fusions (Markus et al., 2011) at microtubule plus ends in 77.2% and 41.4% of cells, respectively (Fig. 1, D and E). In contrast, upon induction of $Num1_{CC}$ overexpression (by growth in galactose-containing media), the number of cells exhibiting Dyn1- and Jnm1-3mCherry plus end foci was reduced by approximately fivefold, to 14.8% and 8.1%, respectively. Fluorescence intensity measurements revealed that those plus ends with Dyn1- and Jnm1-3mCherry foci had significantly fewer molecules of each upon $Num1_{CC}$ overexpression (Fig. 1 F). Coincident with the reduction in plus end dynein and dynactin, we also observed a four- to fivefold increase in the number of cells with Dyn1- and Jnm1-3mCherry foci at SPBs upon $Num1_{CC}$ induction (also see Fig. 4 A, bottom). We observed similar results for Pac11- (dynein intermediate chain) and Dyn3-3mCherry (dynein light-intermediate chain; Fig. S2, A–E). In contrast, overexpression of $Num1_{CC}$ had no effect on the extent of plus end localization of Bik1-3mCherry (CLIP170 homologue), a protein that is required for the plus end targeting of dynein (Fig. S2, F and G; Sheeman et al., 2003). To determine whether there is a cell cycle–regulated component to $Num1_{CC}$-mediated dynein relocalization, we categorized plus end and SPB localization frequencies into the following: G1, preanaphase, and anaphase (as determined by cell and spindle morphology; see Fig. S2 H). Although both G1 and preanaphase cells exhibited an equivalent extent of $Num1_{CC}$-mediated dynein relocalization, we found that anaphase cells were less susceptible to dynein plus end depletion, in spite of a significant enhancement in the prevalence of SPB localized dynein in these cells (Fig. S2 H). These findings are consistent with the higher frequency of dynein plus end localization noted in wild-type anaphase cells (Sheeman et al., 2003; Markus et al., 2009), and they further suggest that the plus end targeting mechanism is more robust at this point of the cell cycle. Collectively, our data indicate that overexpression of $Num1_{CC}$ specifically depletes dynein–dynactin from microtubule plus ends.
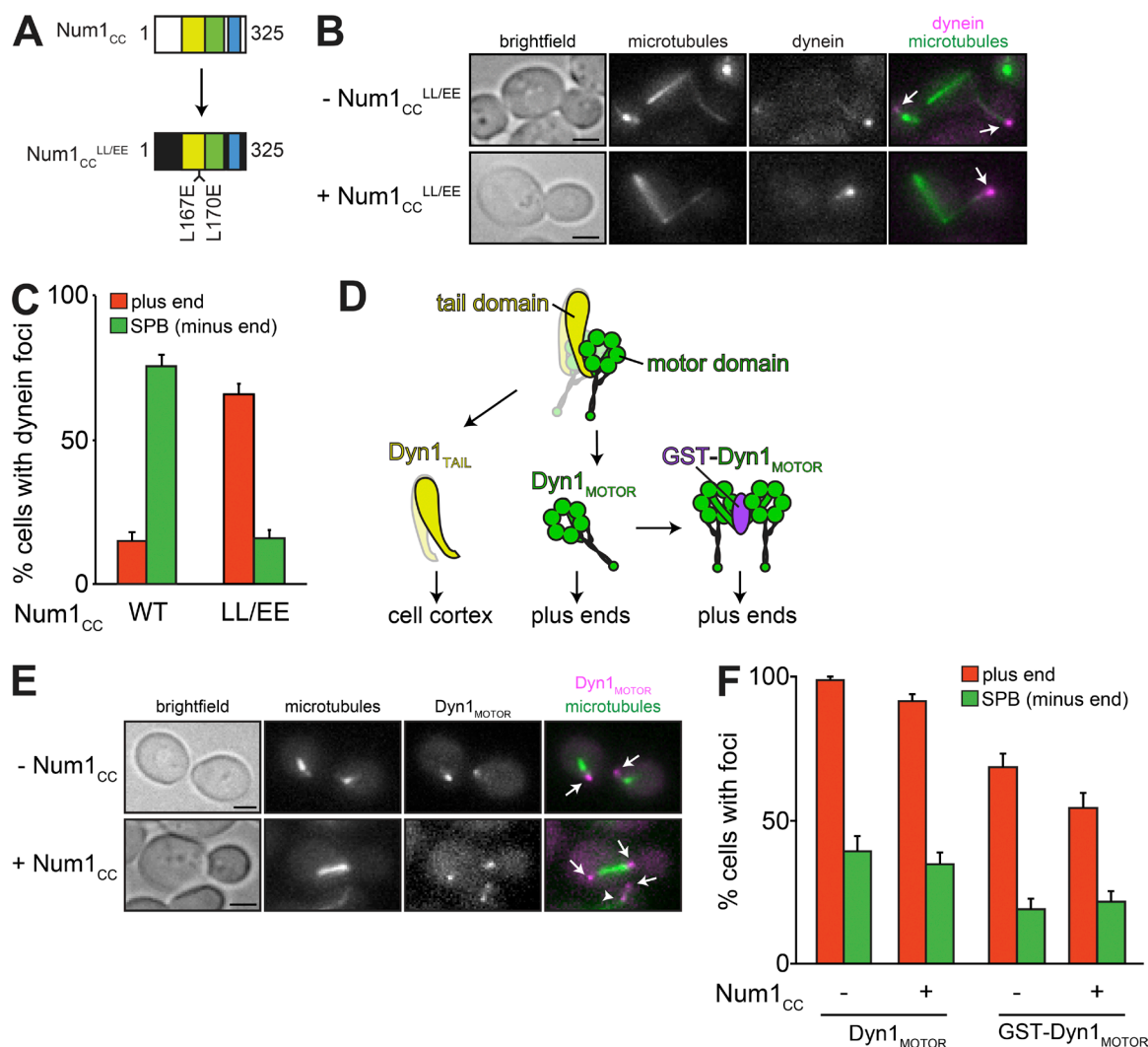
We next wanted to determine whether a Num1-dynein interaction was required for the plus end depletion phenotype. First, we introduced two point mutations within $Num1_{CC}$ (L167E L170E; $Num1_{CC}^{LL/EE}$; Fig. 2 A) that disrupt its interaction with dynein–dynactin but have no effect on Num1 localization or its mitochondria cortical attachment function (Tang et al., 2012).
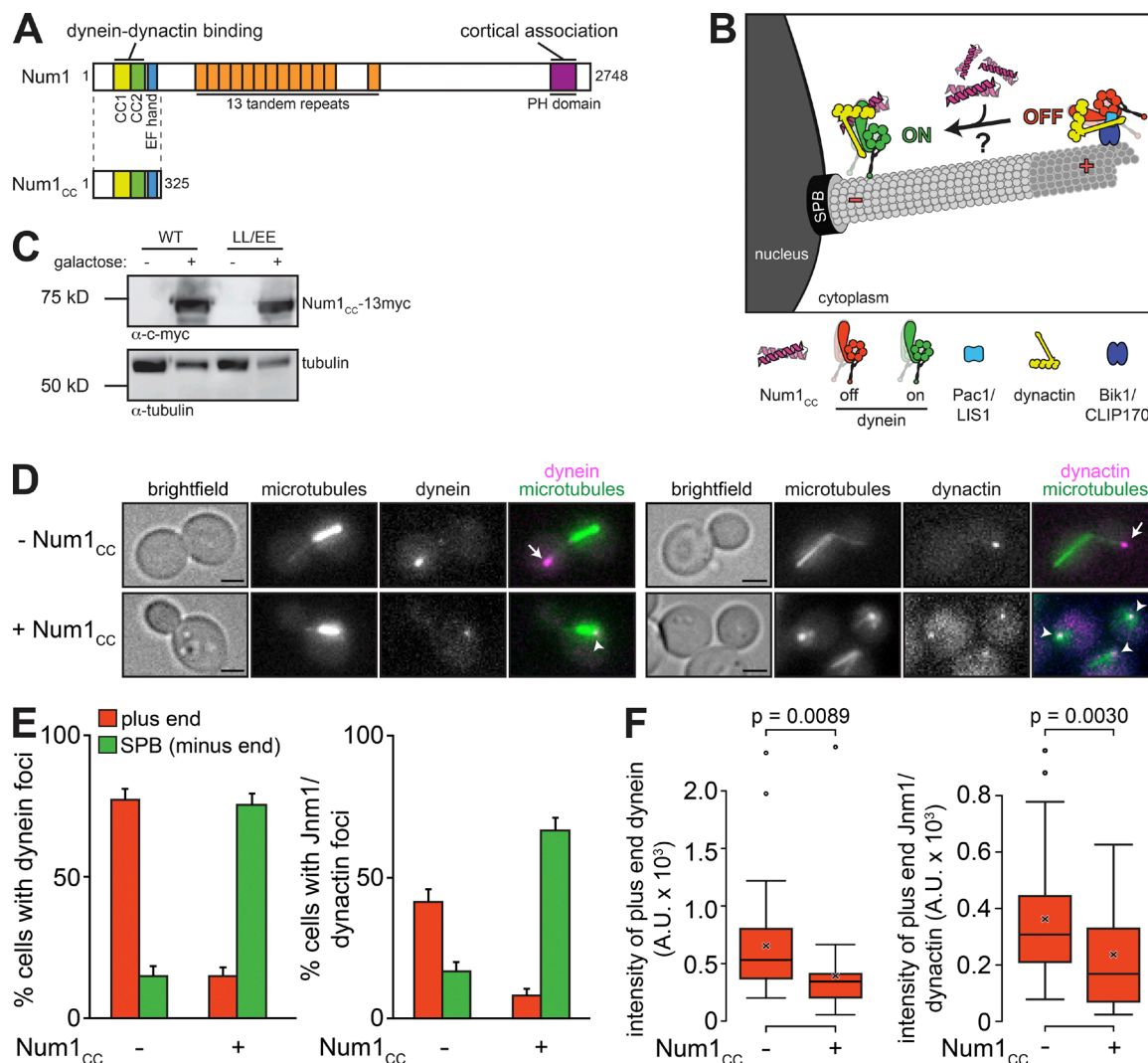
Figure 1. **Overexpression of Num1$_{CC}$ depletes dynein and dynactin from microtubule plus ends.** (A) Schematic representation of Num1 and Num1$_{CC}$ with domain structure indicated (CC1 and CC2, predicted coiled-coil domains; PH, plecktrin homology domain). (B) Diagram depicting experimental design (see text). (C) Western blot of *GAL1p:num1$_{CC}$-13myc* (wild-type or LL/EE mutant) cells grown in the absence or presence of galactose, as indicated, with loading control (anti–α-tubulin). (D) Representative images of *GAL1p:num1$_{CC}$* cells expressing mTurquoise2-Tub1 (α-tubulin) and either Dyn1-3mCherry (left) or Jnm1-3mCherry (right) used for quantitation in E and F. Cells were grown to mid-log phase in SD media supplemented with glucose (uninduced; −Num1$_{CC}$) or galactose plus raffinose (induced; +Num1$_{CC}$). Each image is a maximum-intensity projection of a 2-μm Z-stack of wide-field images. Arrows indicate plus end foci, and arrowheads indicate SPB foci. Bars, 2 μm. (E) The percentage of cells that exhibit plus end (red) or SPB (green) fluorescent foci is plotted for the strains shown in D. Plus end or SPB foci were identified in two-color movies and scored accordingly (see Materials and methods). Error bars represent the standard error of proportion ($n \geq 114$ cells). (F) Box plot of fluorescence intensity values of plus end–associated Dyn1- or Jnm1-3mCherry foci ($n \geq 30$ foci). Whiskers define the range of data, boxes encompass the 25th to 75th quartiles, the line depicts the median value, and the "x" depicts the mean value. See also Video 1 and Figs. S1, S2, and S3.

We found that overexpression of Num1$_{CC}$$^{LL/EE}$ (Fig. 1 C) had no effect on dynein plus end or SPB localization (Fig. 2, B and C), indicating that an intact dynein–dynactin binding surface within Num1$_{CC}$ is required for plus end depletion. Second, we used two dynein motor domain variants (Dyn1$_{MOTOR}$ and GST-Dyn1$_{MOTOR}$) that are sufficient for association with microtubule plus ends but lack the N-terminal tail domain that is required for association with Num1 (Fig. 2 D; Markus et al., 2009). We found that Num1$_{CC}$ overexpression had little effect on the frequency by which monomeric (nonmotile) Dyn1$_{MOTOR}$-3YFP or the dimeric (motile; Reck-Peterson et al., 2006) GST-Dyn1$_{MOTOR}$-3mCherry fragment was observed at plus ends or SPBs (Fig. 2, E and F). Collectively, these data indicate that Num1$_{CC}$-mediated plus end depletion of dynein requires an interaction between dynein and Num1$_{CC}$.

Several lines of evidence indicate that an intact dynein–dynactin complex is required for interaction with Num1. Yeast dynactin deletion mutants exhibit a complete loss of cortical dynein and a higher than normal accumulation of dynein at microtubule plus ends (Lee et al., 2003, 2005). This latter observation is also noted in *num1Δ* mutants (Lee et al., 2003) and is presumed to be attributable to an inability to offload dynein–dynactin to cortical Num1 receptor sites. Finally, a bead-immobilized recombinant Num1$_{CC}$ fragment was sufficient to isolate dynein from cell extracts but was unable to do so from extracts prepared from *nip100Δ* cells (homologue of human dynactin component p150Glued; Tang et al., 2012). To determine whether Num1$_{CC}$ can deplete plus end dynein in the absence of dynactin, we overexpressed Num1$_{CC}$ in *nip100Δ*

Figure 2.   **Interaction between dynein and Num1$_{CC}$ is required for plus end depletion.** (A) Schematic representation of the Num1$_{CC}$$^{LL/EE}$ mutant. (B) Representative images of *GAL1p:num1$_{CC}$$^{LL/EE}$* and *GAL1p:num1$_{CC}$* cells expressing mTurquoise2-Tub1 and Dyn1-3mCherry used for quantitation in C. (C) The percentage of cells that exhibit plus end (red) or SPB (green) fluorescent foci is plotted for the strains overexpressing wild-type (WT) or mutant (LL/EE) Num1$_{CC}$. Error bars represent the standard error of proportion ($n \geq 170$ cells). (D) Diagram depicting dynein N-terminal (tail) and C-terminal (motor) domains and an artificially dimerized GST-Dyn1$_{MOTOR}$ construct (see text). (E) Representative images of *GAL1p:num1$_{CC}$* cells expressing mTurquoise2-Tub1 and Dyn1$_{MOTOR}$-3YFP used for quantitation in F. (F) The percentage of cells that exhibit plus end (red) or SPB (green) fluorescent Dyn1$_{MOTOR}$-3YFP or GST-Dyn1$_{MOTOR}$-3mCherry foci is plotted. Error bars represent the standard error of proportion ($n \geq 87$ cells). All images are maximum-intensity projections of a 2-μm Z-stack of wide-field images. Arrows indicate plus end foci, and the arrowhead indicates the SPB focus. Bars, 2 μm.

cells. We found that Num1$_{CC}$ overexpression reduced the frequency of dynein plus end localization in *nip100Δ* cells to a lesser extent than in *NIP100* cells (Fig. S3, A and B; 38% reduction in *nip100Δ* vs. 81% reduction in *NIP100* cells; compare with Fig. 1 E); however, fluorescence intensity measurements of plus end dynein revealed no significant difference (Fig. S3 C). These data suggest that the ability of dynein to interact with Num1$_{CC}$ is compromised but not abolished in the absence of dynactin.

We next asked whether plus end targeting of dynein is a requisite for Num1$_{CC}$-mediated accumulation of dynein at SPBs. To test this, we deleted either Pac1 or Bik1, both of which are required for dynein plus end targeting (Lee et al., 2003; Sheeman et al., 2003). As expected, neither *pac1Δ* nor *bik1Δ* cells overexpressing Num1$_{CC}$ exhibited plus end dynein foci; in addition, SPB localization of dynein was apparent in only a small number of cells in both mu-

tants, suggesting that the accumulation of dynein at SPBs requires a pool of dynein–dynactin at plus ends from which to draw (Fig. S3, D–G).

Microtubule binding by dynein is required for plus end depletion

If Num1$_{CC}$-mediated redistribution of dynein from plus ends to SPBs is a consequence of activated dynein motility, then we reasoned that a motility-incompetent dynein mutant would remain associated with plus ends in the presence of overexpressed Num1$_{CC}$. To test this, we generated a dynein mutant lacking its microtubule-binding domain (MTBD; Dyn1$_{\Delta MTBD}$; Fig. 3 A). Surprisingly, we found that in the absence of Num1$_{CC}$ induction, Dyn1$_{\Delta MTBD}$ was capable of plus end binding (Fig. 3, B and C, top in B), indicating that dynein associates with plus ends independently of its MTBD, and thus likely through its interaction with Pac1 and Bik1. Furthermore, we found that the
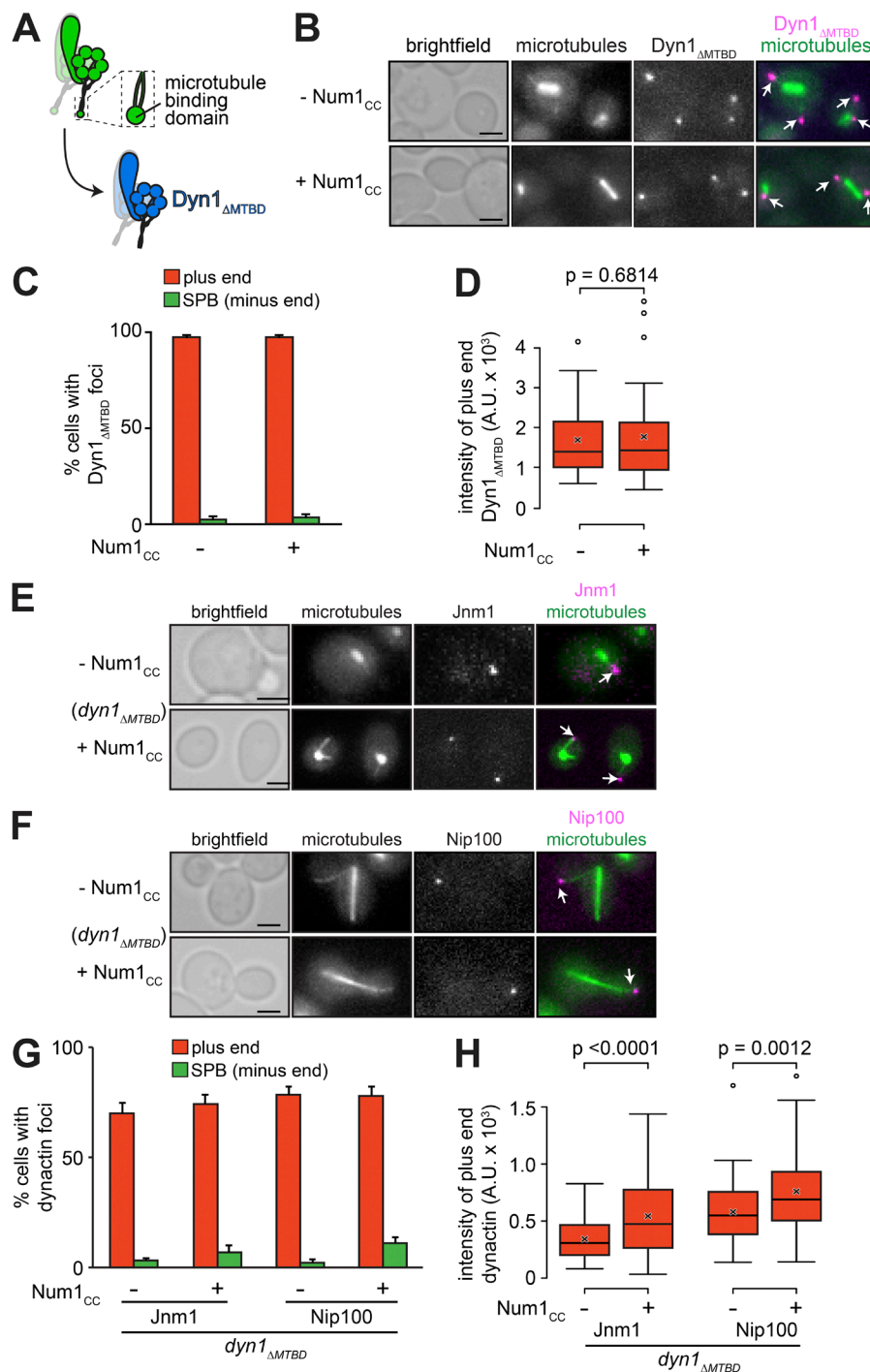
Figure 3. **The dynein MTBD is dispensable for plus end targeting but is required for Num1$_{CC}$-mediated plus end depletion.** (A) Schematic representation of the Dyn1$_{\Delta MTBD}$ mutant. (B) Representative images of *GAL1p:num1$_{CC}$* cells expressing mTurquoise2-Tub1 and Dyn1$_{\Delta MTBD}$-3mCherry used for quantitation in C and D. (C) The percentage of cells that exhibit plus end (red) or SPB (green) Dyn1$_{\Delta MTBD}$-3mCherry foci is plotted for cells shown in B. Error bars represent the standard error of proportion ($n \geq 126$ cells). (D) Box plot of fluorescence intensity values of plus end–associated Dyn1$_{\Delta MTBD}$-3mCherry ($n \geq 40$ foci). (E and F) Representative images of *GAL1p:num1$_{CC}$ dyn1$_{\Delta MTBD}$* cells expressing mTurquoise2-Tub1 and either Jnm1- (E) or Nip100-3mCherry (F) used for quantitation in G and H. (G) The percentage of *dyn1$_{\Delta MTBD}$* cells that exhibit plus end or SPB Jnm1- or Nip100-3mCherry foci is plotted for *GAL1p:num1$_{CC}$* cells grown in glucose (−Num1$_{CC}$) or galactose (+Num1$_{CC}$; $n \geq 100$ cells). (H) Box plot of fluorescence intensity values of plus end–associated Jnm1- or Nip100-3mCherry ($n \geq 56$ foci). For all box plots, whiskers define the range of data, boxes encompass the 25th to 75th quartiles, the line depicts the median value, and the "x" depicts the mean value. All images are maximum-intensity projections of a 2-µm Z-stack of widefield images. Arrows indicate plus end foci. Bars, 2 µm. See also Fig. S5.

extent of plus end localization of Dyn1$_{\Delta MTBD}$ was greater than wild-type Dyn1 (26% increase in frequency; 148% increase in intensity; P < 0.0001), whereas its SPB localization was lower (Fig. 3, C and D; compare with Fig. 1, E and F). These data suggest that SPB localization of dynein in wild-type cells may be attributable to minus end–directed motility of active dynein motors. Consistent with our hypothesis, upon induction of Num1$_{CC}$ overexpression, Dyn1$_{\Delta MTBD}$ localization to plus ends and SPBs remained unchanged (Fig. 3, C and D), suggesting that Num1$_{CC}$-mediated depletion of dynein from plus ends and accumulation at SPBs both require dynein motility.

Num1$_{CC}$ has only a modest effect on dynein–dynactin interaction at plus ends

In contrast to yeast dynein, metazoan dynein exhibits mostly nonprocessive, diffusive motility in single-molecule assays (Miura et al., 2010; McKenney et al., 2014; Schlager et al., 2014). A family of coiled-coil–containing adaptor proteins that recruit dynein and dynactin to various cellular sites was recently shown to be sufficient to activate processive single-molecule motility by stably linking dynein to dynactin (McKenney et al., 2014; Schlager et al., 2014). Like these adaptor proteins, Num1 interacts only with intact dynein–dynactin complexes

through its coiled-coil domain (Splinter et al., 2012; Tang et al., 2012). Although dynein recruits dynactin to plus ends in a Num1-independent manner, dynactin is present at substoichiometric amounts relative to dynein (approximately three dynein to one dynactin; Markus et al., 2011). Thus, we reasoned that $Num1_{CC}$ may activate dynein motility by enhancing the dynein–dynactin interaction at plus ends. To test this, we assessed the extent by which $Num1_{CC}$ affects dynein-mediated recruitment of dynactin to plus ends. For these experiments, we used $dyn1_{\Delta MTBD}$ mutant cells, in which dynein remains associated at plus ends in spite of $Num1_{CC}$ overexpression (see Fig. 3, B–D). We found that $Num1_{CC}$ overexpression had no effect on the frequency of observing plus end–localized dynactin (i.e., Jnm1- or Nip100-3mCherry; Fig. 3, E–G); however, the fluorescence intensities of both Jnm1 and Nip100 at plus ends were modestly, but significantly, increased (Fig. 3 H; 58.9% and 30.9%, respectively; P ≤ 0.0012), suggesting that $Num1_{CC}$ may in fact enhance or stabilize the dynein–dynactin interaction. However, given the small apparent change in dynein–dynactin interaction at plus ends, and the observation that yeast dynein processivity enhancement by dynactin does not require additional factors in vitro (i.e., Num1; Kardon et al., 2009), it is unclear whether stabilization of the dynein–dynactin interaction is the mechanism by which Num1 functions to activate dynein motility. For these reasons, we explored an alternative hypothesis.

Overexpression of Num1$_{CC}$ reduces colocalization of dynein and Pac1

Cells in which Pac1 is deleted exhibit a complete loss of plus end dynein (Lee et al., 2003; Markus et al., 2009), similar to our observations of cells overexpressing $Num1_{CC}$. We hypothesized that $Num1_{CC}$ may deplete dynein from plus ends by interfering with dynein-Pac1 binding. To test this, we assessed localization of a functional Pac1-3mCherry fusion (Markus et al., 2011) in cells overexpressing $Num1_{CC}$. As we observed for dynein and dynactin, Pac1-3mCherry foci were depleted from microtubule plus ends upon $Num1_{CC}$ overexpression (Fig. 4, A and B), consistent with their codependence for plus end targeting (Markus et al., 2011). However, in contrast to dynein and dynactin, the fraction of cells exhibiting Pac1-3mCherry foci at SPBs was reduced with respect to cells not expressing $Num1_{CC}$, suggesting that dynein localizes at SPBs without Pac1 upon $Num1_{CC}$ overexpression. This reduction in localization was not due to a decrease in Pac1 protein expression or stability, as indicated by immunoblotting (Fig. 4 D). Consistent with a $Num1_{CC}$-mediated reduction in the dynein-Pac1 interaction, we found that the fraction of Dyn1-3YFP and Pac1-3mCherry foci that colocalized (either SPB or plus end) was reduced upon induction of $Num1_{CC}$ (from 59.6% to 26.2%; Fig. 4 E), whereas the fraction of Dyn1-3YFP foci alone (i.e., not colocalized with Pac1) increased (from 28.3% to 62.3%). These data suggest that overexpression of $Num1_{CC}$ may disrupt plus end binding of dynein–dynactin by interfering with the dynein-Pac1 interaction.

We next wanted to determine whether the reduction in Pac1-dynein colocalization was a direct consequence of $Num1_{CC}$-mediated Pac1-dynein dissociation, or whether it was a secondary consequence of dynein plus end depletion. To distinguish between these two possibilities, we ectopically targeted dynein to the plasma membrane using an exogenous pleckstrin homology (PH) domain, and we assessed the degree of colocalization of Pac1 with cortical PH-Dyn1 in the presence of either $Num1_{CC}^{LL/EE}$ or $Num1_{CC}$. We found that the PH domain was

sufficient to target dynein (Fig. 4 F and Fig. S4 A) and dynactin (i.e., Jnm1; Fig. S4 B) to the cell cortex in cells lacking cortical Num1. Interestingly, we found a greater frequency of cortical PH-Dyn1-3mCherry foci in $Num1_{CC}$-overexpressing cells than in either $Num1_{CC}^{LL/EE}$-overexpressing cells (45.5% vs. 13.9%, respectively) or $NUM1$ cells (21.3%; not depicted). In addition, we noted that $Num1_{CC}$-overexpressing cells exhibited larger cortical patches than either wild-type $NUM1$ or $Num1_{CC}^{LL/EE}$-overexpressing cells (Fig. S4 A; data not depicted). These data suggest that PH-Dyn1-$Num1_{CC}$ complexes may be oligomerizing at the cell cortex, which is consistent with the previously described role for the $Num1_{CC}$ domain in the assembly of higher-order cortical patches (Tang et al., 2012). In cells overexpressing $Num1_{CC}^{LL/EE}$, Pac1-3YFP colocalized with 65.3% of cortical PH-Dyn1-3mCherry foci; however, upon overexpression of $Num1_{CC}$, only 29.1% of PH-Dyn1-3mCherry foci contained Pac1-3YFP fluorescence (Fig. 4 G). Fluorescence intensity measurements also revealed a significant reduction in the number of Pac1 molecules associated with cortical PH-dynein patches (Fig. 4 H). In contrast, we noted no significant change in either the frequency or intensity of colocalized dynactin (i.e., Jnm1; Fig. 4, I and J; and Fig. S4 B). These data support the notion that $Num1_{CC}$ disrupts the dynein-Pac1 interaction, thereby leading to the plus end depletion phenotype.

An enhanced Pac1 affinity mutant of dynein or Pac1 overexpression reduces the extent of Num1$_{CC}$-mediated plus end depletion of dynein

If a $Num1_{CC}$-mediated Pac1 unbinding event is the cause for plus end depletion of dynein–dynactin complexes, we reasoned that we could reduce the extent of $Num1_{CC}$-mediated dynein depletion from microtubule plus ends by two different means: (a) enhancing the affinity of dynein for Pac1, or (b) overexpression of Pac1. To test the former, we used a yeast strain expressing a well-characterized, motility-competent dynein mutant ($Dyn1_{HL3}$) that exhibits higher affinity for Pac1 than wild-type dynein (Fig. 5 A; Markus and Lee, 2011). We predicted that $Dyn1_{HL3}$ and Pac1 would be less susceptible to $Num1_{CC}$-mediated plus end depletion as a result of their higher affinity. Consistent with our hypothesis, induction of $Num1_{CC}$ overexpression reduced the frequency of observing $Dyn1_{HL3}$-3YFP and Pac1-3mCherry plus end foci by 40% and 22%, respectively (Fig. 5, B and C), much less than what we observed in wild-type $DYN1$ cells (respective 81% and 67% reduction; compare with Fig. 1 E and Fig. 4 B). Fluorescence intensity measurements revealed no significant change in the number of $Dyn1_{HL3}$ or Pac1 molecules at plus ends upon $Num1_{CC}$ overexpression (Fig. 5 D). Thus, both Pac1 and $Dyn1_{HL3}$ are less susceptible to plus end depletion by $Num1_{CC}$ overexpression in $dyn1_{HL3}$ cells.

To test whether overexpression of Pac1 could rescue plus end depletion, we replaced the native $PAC1$ promoter with the $GAL1$ promoter, which is sufficient to induce >10-fold higher Pac1 expression levels compared with wild-type cells (Markus et al., 2011). To establish a baseline for Pac1 overexpression–mediated enhancement of dynein plus end targeting, we first assessed dynein localization in cells overexpressing Pac1 and $Num1_{CC}^{LL/EE}$, the latter of which has no discernible effect on dynein targeting (see Fig. 2, B and C). In these cells, we observed an increase in both frequency and mean fluorescence intensity of plus end dynein by 44% and 170%, respectively (Fig. 6, B and D), compared with cells overexpressing $Num1_{CC}^{LL/EE}$ and
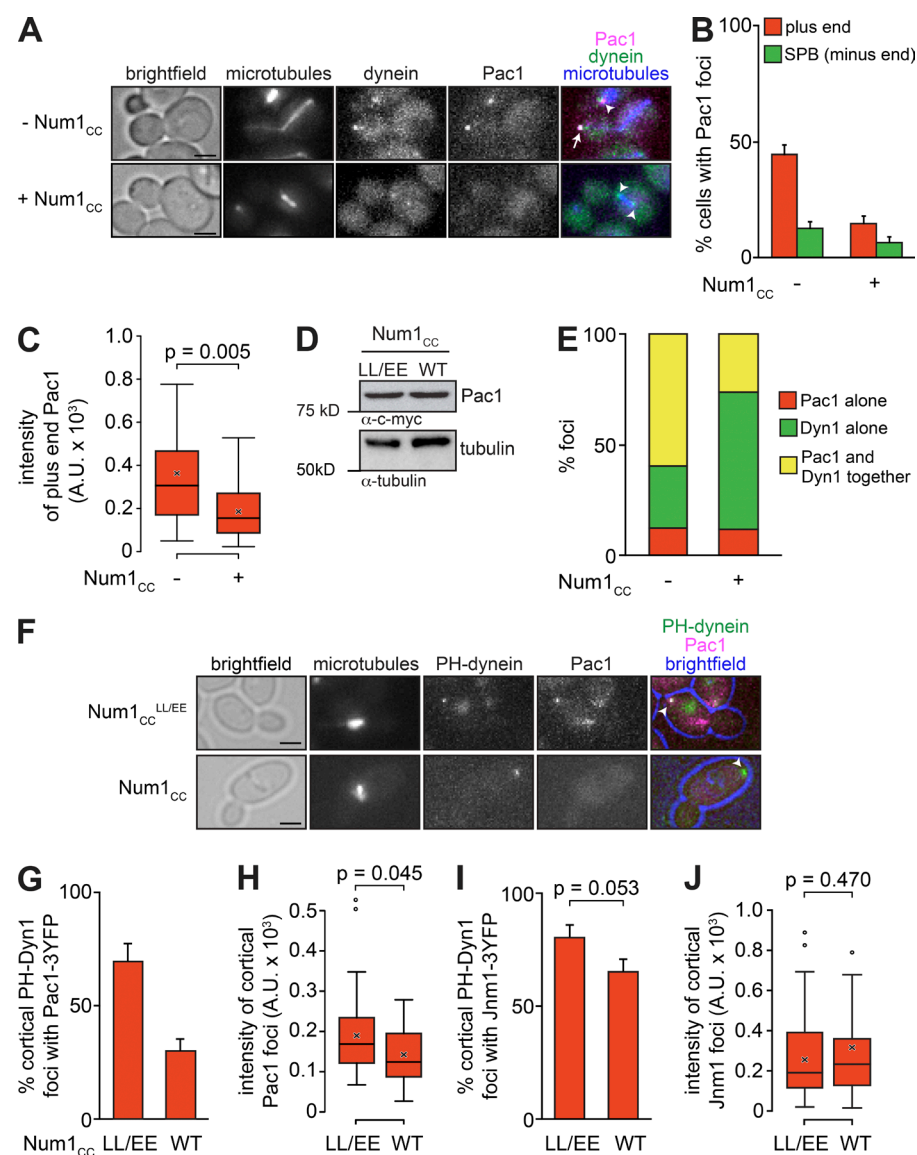
Figure 4. **Overexpression of Num1$_{CC}$ depletes Pac1 from plus ends and disrupts dynein-Pac1 interaction.** (A) Representative images of *GAL1p:num1$_{CC}$* cells expressing mTurquoise2-Tub1, Pac1-3mCherry, and Dyn1-3YFP used for quantitation in B, C, and E. The arrow indicates the plus end focus, and arrowheads indicate SPB foci. (B) The percentage of cells that exhibit plus end (red) or SPB (green) fluorescent Pac1-3mCherry foci is plotted for the cells shown in A. Error bars represent the standard error of proportion ($n \geq 122$ cells). (C) Box plot of fluorescence intensity values of plus end–associated Pac1-3mCherry ($n \geq 26$ foci). (D) Western blot of Pac1-13myc–expressing *GAL1p:num1$_{CC}$* or *GAL1p:num1$_{CC}^{LL/EE}$* cells (as indicated) grown in galactose-containing media with loading control (anti–α-tubulin). (E) The extent of Pac1-3mCherry and Dyn1-3YFP colocalization is plotted for the indicated cells ($n \geq 61$ fluorescent foci). (F) Representative images of *GAL1p:PH-DYN1-3mCherry* cells expressing Pac1-3YFP and either Num1$_{CC}$ or Num1$_{CC}^{LL/EE}$. Arrowheads indicate cortical foci. (G and I) The percentage of cortical PH-Dyn1-3mCherry foci that colocalize with either Pac1-3YFP ($n \geq 49$ foci; G) or Jnm1-3YFP ($n \geq 55$ foci; I) is plotted for cells expressing either Num1$_{CC}$ or Num1$_{CC}^{LL/EE}$. (H and J) Box plot of fluorescence intensity values for either cortical Pac1-3YFP ($n \geq 25$ foci; H) or Jnm1-3YFP foci ($n \geq 44$ foci; one outlier was omitted from the plot for display purposes only; J). For all box plots, the whiskers define the range of data, boxes encompass the 25th to 75th quartiles, the line depicts the median value, and the "x" depicts the mean value. All images are maximum-intensity projections of a 2-μm Z-stack of wide-field images. Bars, 2 μm. See also Fig. S4. WT, wild type.

expressing native levels of Pac1. In comparison, overexpression of Pac1 and wild-type Num1$_{CC}$ reduced the frequency of plus end dynein by 47% (P < 0.0001; compare *GAL1p:PAC1* with *GAL1p:PAC1 num1$_{CC}$*), whereas the mean fluorescence intensity was not reduced significantly (30%; P = 0.1636; Fig. 6, B and D). These values are significantly less than the respective 78% and 37% reduction in frequency and intensity we observed when Num1$_{CC}$ alone was overexpressed (compared with Num1$_{CC}^{LL/EE}$; Fig. 6, C and E). Thus, Pac1 overexpression reduces the extent by which Num1$_{CC}$ depletes dynein from microtubule plus ends.

If Num1$_{CC}$ depletes dynein from plus ends by inducing Pac1 release, then we reasoned that enhancing dynein plus end targeting by a Pac1-independent means would not be able to rescue plus end depletion to the same extent as Pac1 overexpression. To test this, we overexpressed Kip2, a kinesin-7 family member that affects steady-state microtubule length (see Fig. 6 A, bottom) and plays a role in transporting dynein to microtubule plus ends (Carvalho et al., 2004; Markus et al., 2009; Roberts et al., 2014). As with Pac1, we first established a baseline by which Kip2 overexpression enhances dynein plus end localization by imaging Dyn1-3mCherry in *GAL1p:KIP2*

GAL1p:num1$_{CC}^{LL/EE}$ cells. Consistent with a role for Kip2 in transporting dynein away from minus ends and toward plus ends, overexpression of Kip2 enhanced the frequency of dynein plus end targeting by 19% and reduced the frequency of SPB targeting by 83% (P = 0.0019; Fig. 6 B). Fluorescence intensity measurements revealed a robust 147% increase in the number of dynein molecules per plus end (Fig. 6 D). When both Kip2 and wild-type Num1$_{CC}$ were overexpressed, the frequency and mean fluorescence intensity of plus end dynein was reduced by 59% (P < 0.0001) and 63% (P = 0.0012), respectively, compared with *GAL1p:KIP2 GAL1p:num1$_{CC}^{LL/EE}$* cells (Fig. 6, B–E). The extent by which Kip2 overexpression reduces Num1$_{CC}$-mediated plus end dynein depletion is therefore less than that of Pac1. Collectively, these data are consistent with our hypothesis, and they suggest that Num1$_{CC}$ and Pac1 are competing for binding to dynein–dynactin complexes. It is interesting to note that Pac1 binds to dynein within the C-terminal motor domain (Reck-Peterson et al., 2006; Markus et al., 2009; Huang et al., 2012; Toropova et al., 2014), whereas Num1 associates with dynein via the N-terminal tail domain (Markus et al., 2009). Thus, interference with Dyn1-Pac1 binding by Num1$_{CC}$ likely occurs by an allosteric mechanism.
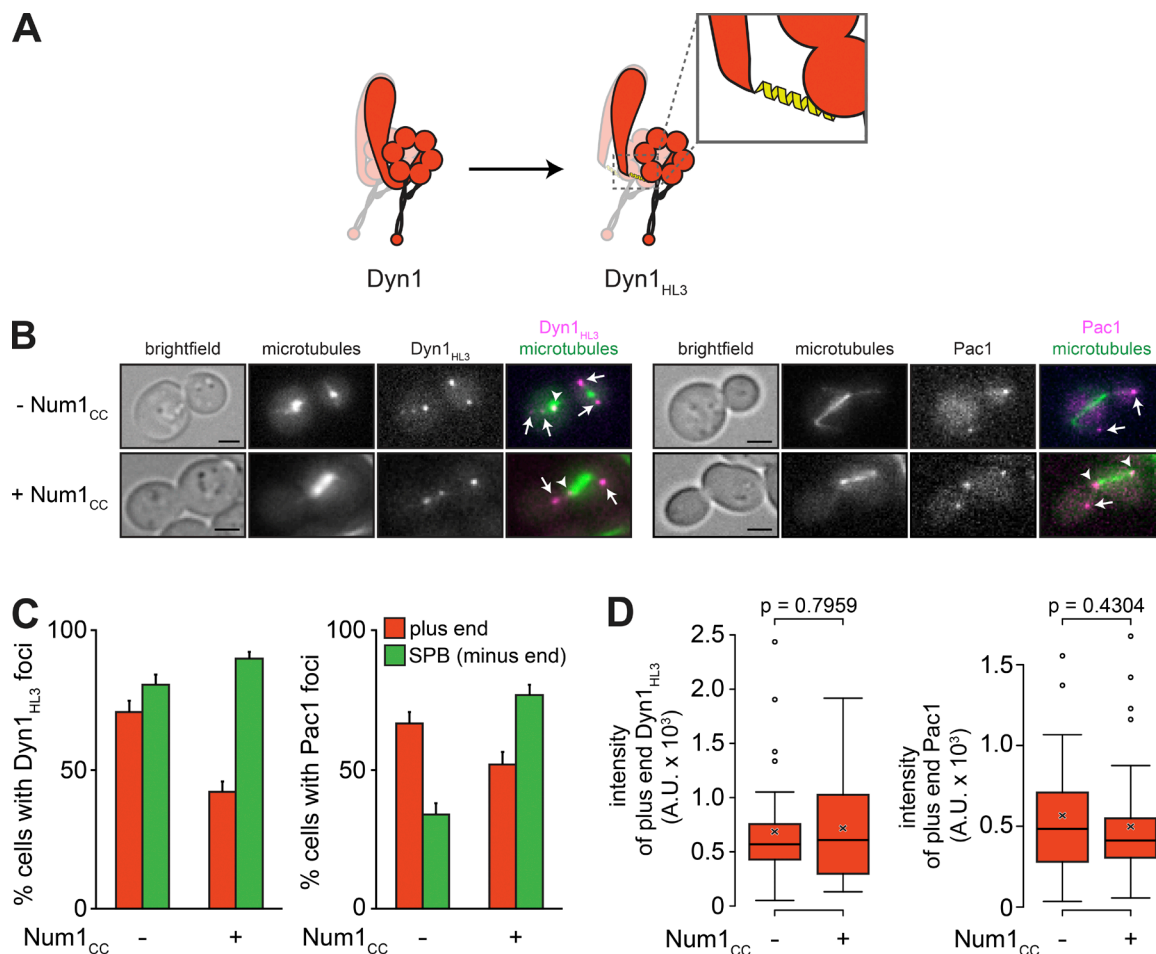
Figure 5. **Dyn1$_{HL3}$ is less susceptible to Num1$_{CC}$-mediated plus end depletion.** (A) Diagram depicting the Dyn1$_{HL3}$ high Pac1 affinity mutant, in which a helical linker has been inserted between the dynein tail and motor domains (Markus and Lee, 2011). (B) Representative images of *GAL1p:num1$_{CC}$* cells expressing mTurquoise2-Tub1 and either Dyn1$_{HL3}$-3YFP (left) or Dyn1$_{HL3}$ and Pac1-3mCherry (right) used for quantitation in C and D. Each image is a maximum-intensity projection of a 2-µm Z-stack of wide-field images. Arrows indicate plus end foci, and arrowheads indicate SPB foci. Bars, 2 µm. (C) The percentage of cells that exhibit plus end (red) or SPB (green) fluorescent Dyn1$_{HL3}$-3YFP (left) or Pac1-3mCherry (right) foci is plotted for the cells shown in B. Error bars represent the standard error of proportion ($n \geq 119$ cells). (D) Box plot of fluorescence intensity values of plus end–associated Dyn1$_{HL3}$-3YFP or Pac1-3mCherry ($n \geq 33$ foci). Whiskers define the range of data, boxes encompass the 25th to 75th quartiles, the line depicts the median value, and the "x" depicts the mean value. See also Fig. S5.

Num1$_{CC}$ colocalizes with dynein–dynactin

Previous data indicate that Num1$_{CC}$ interacts with dynein at SPBs and is found in the cytoplasm as bright foci (presumably aggregates; see Fig. S5, A and B, open arrows and cytoplasm, respectively; Tang et al., 2012). We found that localization of Num1$_{CC}$ to the SPB is largely dependent on dynein, and more specifically, the MTBD of dynein (Fig. S5, A and B). Furthermore, cells in which dynein plus end targeting is restored—by overexpression of Pac1, deletion of the dynein MTBD, or use of Dyn1$_{HL3}$—exhibit Num1$_{CC}$ at plus ends, albeit at a low frequency (Fig. S5, A–C). These data indicate that Num1$_{CC}$ can bind plus end dynein (as well as the Dyn1$_{\Delta MTBD}$ and Dyn1$_{HL3}$ mutants) and suggest that Num1 and Pac1 binding to dynein is not entirely mutually exclusive. The latter is consistent with the observation that Dyn1$_{HL3}$-Pac1 complexes can offload together to Num1 cortical sites (Markus and Lee, 2011).
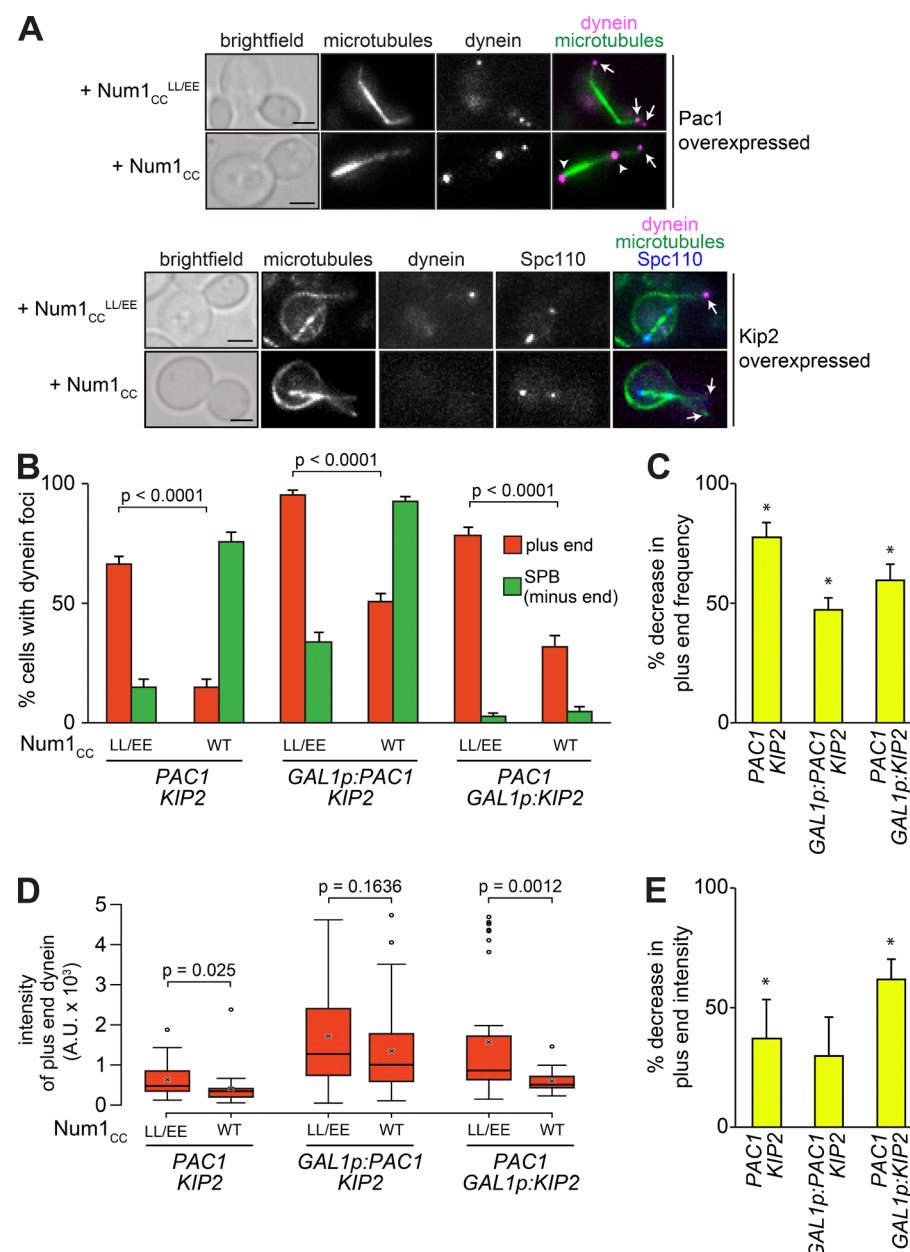
Direct observation of minus end–directed motion of dynein along astral microtubules

In budding yeast, dynein is targeted to microtubule plus ends by two distinct mechanisms: (a) direct recruitment from the cytoplasm, and (b) Kip2-mediated plus end–directed transport along astral microtubules (Carvalho et al., 2004; Markus et al., 2009). Evidence of the latter is apparent by the movement of fluorescent dynein speckles along astral microtubules toward plus ends (Fig. 7 A and Video 2; Markus et al., 2009). In budding yeast, dynein is never observed moving in the opposite direction—toward the minus ends of astral microtubules. Minus end–directed activity is only apparent when cortically anchored dynein motors move the spindle through interactions with astral microtubules. If depletion of dynein–dynactin from microtubule plus ends is a consequence of these motors being switched "on," then we reasoned that cells overexpressing Num1$_{CC}$ would exhibit dynein molecules moving in a directed manner toward the minus ends of astral microtubules, as was recently observed in fission yeast expressing a Mcp5$_{\Delta PH}$ (Num1 homologue) fragment (Ananthanarayanan et al., 2013).

In uninduced cells (i.e., not expressing any Num1$_{CC}$) or in those induced to express Num1$_{CC}$$^{LL/EE}$, only plus end–directed motility of dynein (or dynein$_{\Delta MTBD}$) molecules was ever observed (Fig. 7 A and Video 2). We were unable to observe minus end–directed motility of dynein molecules
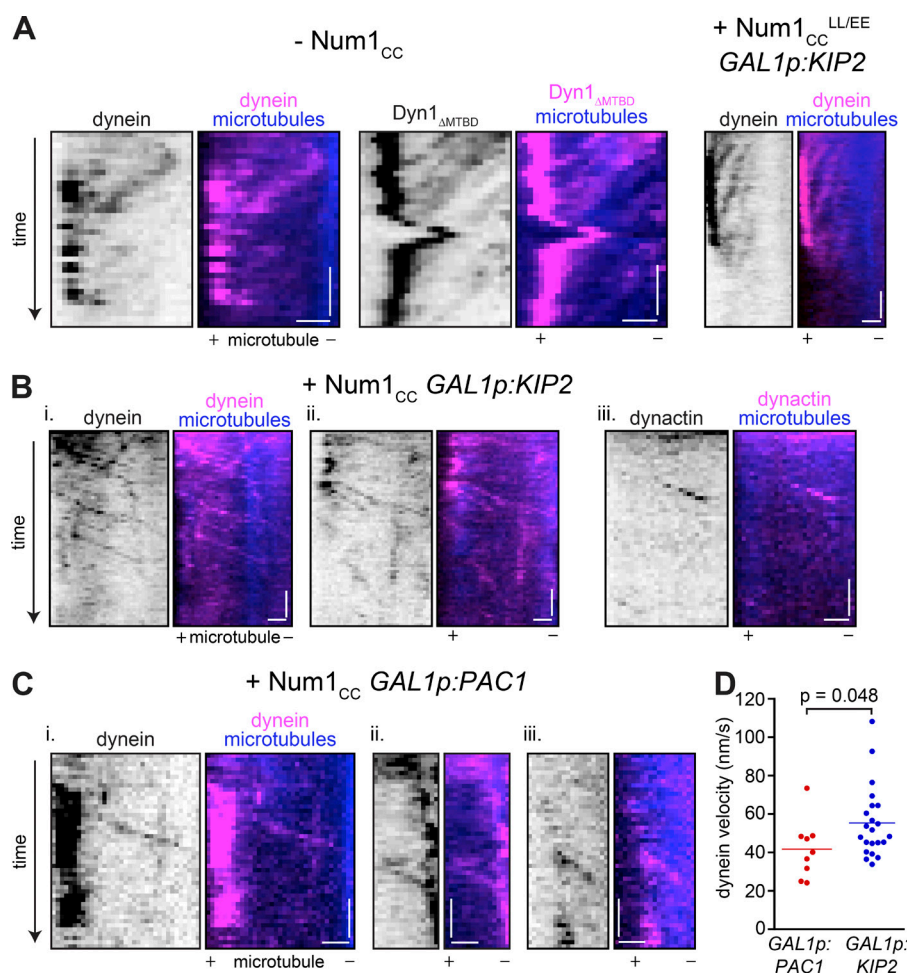
Figure 6. **Overexpression of Pac1 reduces the extent by which Num1$_{CC}$ depletes plus end dynein.** (A) Representative images of cells expressing mTurquoise2-Tub1, Dyn1-3mCherry, either Num1$_{CC}$ or Num1$_{CC}$$^{LL/EE}$, and either overexpressing Pac1 or Kip2, as indicated. Because of the distorted spindle phenotype in Kip2-overexpressing cells, Spc110-Venus was used to mark SPBs. All cells were grown in galactose-containing media to induce overexpression of Pac1, Kip2, Num1$_{CC}$, or Num1$_{CC}$$^{LL/EE}$, as indicated. Each image is a maximum-intensity projection of a 2-μm Z-stack of wide-field images. For the top row (Pac1 overexpressed), arrows indicate plus end foci, and arrowheads indicate SPB foci. For the bottom row (Kip2 overexpressed), arrows indicate plus ends with or without foci. Bars, 2 μm. (B) The percentage of cells that exhibit plus end (red) or SPB (green) Dyn1-3mCherry foci is plotted for cells shown in A and for cells shown in Figs. 1 D and 2 B. Error bars represent the standard error of proportion ($n \geq 113$ cells). (C) Extent by which Num1$_{CC}$ overexpression reduced the frequency of observing dynein plus end foci compared with the respective *PAC1 KIP2* isogenic parent strain overexpressing Num1$_{CC}$$^{LL/EE}$. Asterisks indicate a statistically significant percent decrease (see B for P values). (D) Box plot of fluorescence intensity values of plus end–associated Dyn1-3mCherry ($n \geq 31$ foci). Whiskers define the range of data, boxes encompass the 25th to 75th quartiles, the line depicts the median value, and the "x" depicts the mean value. (E) Extent by which Num1$_{CC}$ overexpression reduced the number of dynein molecules (i.e., fluorescence intensity) at plus ends compared with the isogenic *PAC1 KIP2* parent strain overexpressing Num1$_{CC}$$^{LL/EE}$. Asterisks indicate a statistically significant percent decrease (see D for P values). See also Fig. S5. WT, wild type.

in cells overexpressing Num1$_{CC}$, likely because of the robust depletion of dynein from microtubule plus ends in these cells. Thus, we chose to focus on cells in which Num1$_{CC}$-mediated depletion of dynein plus end binding was partially restored: *GAL1p:KIP2* and *GAL1p:PAC1* cells. Strikingly, we observed numerous instances of minus end–directed motility of dynein in cells overexpressing Kip2 or Pac1 in addition to Num1$_{CC}$ (Fig. 7, B and C; Fig. S5 D; Video 3; and Video 4). The mean velocity of minus end–directed dynein molecules along astral microtubules in *GAL1p:KIP2* cells was slightly higher than that in *GAL1p:PAC1* cells (55.3 nm/s, $n = 22$; vs. 41.7 nm/s, $n = 9$; Fig. 7 D); however, the values from both strains were very similar to the velocity of single molecules of purified dynein (∼70–100 nm/s; Reck-Peterson et al., 2006; Markus and Lee, 2011; Huang et al., 2012) and dynein-mediated spindle movements in this organism

(41 nm/s; Markus et al., 2011). Thus, overexpression of Num1$_{CC}$ depletes dynein from microtubule plus ends by activating its minus end–directed motility.

Although we were able to see Num1$_{CC}$-mediated minus end motility of dynactin (Jnm1-3YFP) in *GAL1p:KIP2* cells (Fig. 7 B, iii), we were unable to observe examples of either Pac1 or Num1$_{CC}$ moving toward the minus ends. The reason for the latter is unclear but may be a result of disengagement of Num1$_{CC}$ from dynein subsequent to activation. Taken together with our other observations (i.e., the lack of Pac1 accumulation at SPBs in Num1$_{CC}$-overexpressing cells, the reduced colocalization of Dyn1 and Pac1 in *DYN1* and *PH-DYN1* cells, and the ability of Pac1 overexpression to rescue Dyn1 plus end targeting), the apparent lack of minus end–directed Pac1 molecules further suggests that Num1$_{CC}$ activates plus end dynein by relieving Pac1-mediated inhibition.

A - Num1$_{CC}$

dynein | dynein microtubules | Dyn1$_{\Delta MTBD}$ | Dyn1$_{\Delta MTBD}$ microtubules

+ Num1$_{CC}$$^{LL/EE}$ *GAL1p:KIP2*

dynein | dynein microtubules

+ microtubule −

B + Num1$_{CC}$ *GAL1p:KIP2*

i. dynein | dynein microtubules | ii. | iii. dynactin | dynactin microtubules

+ microtubule −

C + Num1$_{CC}$ *GAL1p:PAC1*

i. dynein | dynein microtubules | ii. | iii.

+ microtubule −

D p = 0.048

dynein velocity (nm/s)

GAL1p: PAC1 | *GAL1p: KIP2*

Figure 7. **Direct observation of Num1$_{CC}$-mediated minus end motility of dynein and dynactin.** (A) Example kymographs of plus end–directed motility of dynein molecules along astral microtubules observed in uninduced *GAL1p:num1$_{CC}$* cells (left; –Num1$_{CC}$) or in cells overexpressing Num1$_{CC}$$^{LL/EE}$ and Kip2 (right). (B and C) Example kymographs depicting minus end–directed motility of dynein or dynactin (i.e., Jnm1) along astral microtubules in cells overexpressing Num1$_{CC}$ and either Kip2 (B) or Pac1 (C). Kymographs were generated from time-lapse images acquired using highly inclined and laminated optical sheet microscopy (see Materials and methods). Bars: (vertical) 1 min; (horizontal) 1 µm. (D) Velocity values for minus end–directed dynein runs observed in either Pac1- or Kip2-overexpressing cells. See also Fig. S5 and Videos 2 and 3.

Discussion

When purified from various sources, including budding yeast and animal tissue, dynein motors are active as apparent from ATPase and microtubule gliding assays. Yeast dynein requires no additional factors for processive single-molecule motility (Reck-Peterson et al., 2006), whereas dynein isolated from animal tissue requires a combination of dynactin and various adaptor proteins that link dynein to dynactin (McKenney et al., 2014; Schlager et al., 2014). This latter phenomenon helps explain how dynein activity is recruited to different vesicular or organellar compartments in animal cells, and thus how dynein activity is regulated with spatial precision. For instance, one of these adaptors, BicD2, binds to Rab6 on various vesicular cargoes, and thereby recruits dynein–dynactin complexes, which allows for minus end–directed movements of these vesicular cargoes (Matanis et al., 2002). Although mechanistically distinct, we have identified a similar mechanism at play in budding yeast. Specifically, Num1-mediated recruitment of dynein–dynactin complexes to the cell cortex is sufficient to (a) anchor dynein–dynactin complexes at their site of activity, and (b) activate dynein for its spindle orientation function. Unlike animal cells, however, association with dynactin is not sufficient to activate dynein motility in yeast cells. Rather, our studies indicate that a Num1-mediated Pac1 dissociation event is responsible for switching dynein from being off at microtubule plus ends to on at the cell cortex.

Our results revealed a small but significant Num1$_{CC}$-mediated enhancement in the apparent dynein–dynactin inter-

action at plus ends (see Fig. 3 H). Although this effect appears to be minor compared with that of Num1$_{CC}$ on the dynein-Pac1 interaction, it is possible that, like the human adaptor proteins (e.g., BicD2 and Spindly), Num1 also plays a role in stabilizing the dynein–dynactin complex. If so, it may be that Num1 may further promote dynactin-mediated processivity enhancement of dynein in a manner reflective of the human adaptor proteins (McKenney et al., 2014; Schlager et al., 2014). Future studies will be needed to directly test this in a reconstituted system.

Although dynactin does not activate yeast dynein motility, per se, it is interesting to note that dynein–dynactin binding is a rate-limiting step during the dynein offloading process. Quantitative fluorescence microscopy revealed a threefold excess of dynein relative to dynein–dynactin complexes at microtubule plus ends (Markus et al., 2011). Given the reliance of dynein on dynactin for offloading to Num1 receptor sites (Lee et al., 2003), the limiting nature of dynactin at plus ends effectively restricts dynein pathway activity by limiting the number of cortical dynein–dynactin complexes. Increasing the number of intact dynein–dynactin complexes at plus ends by deletion of She1, which regulates their interaction in vivo (Woodruff et al., 2009), results in an increased number of cortical dynein–dynactin complexes, as well as enhanced dynein pathway activity (Markus et al., 2011). Thus, through mechanistically distinct processes, dynactin effectively activates dynein-mediated processes both in animal and yeast cells.

It is well established that Pac1 plays a central role in targeting dynein–dynactin to microtubule plus ends in yeast (Lee
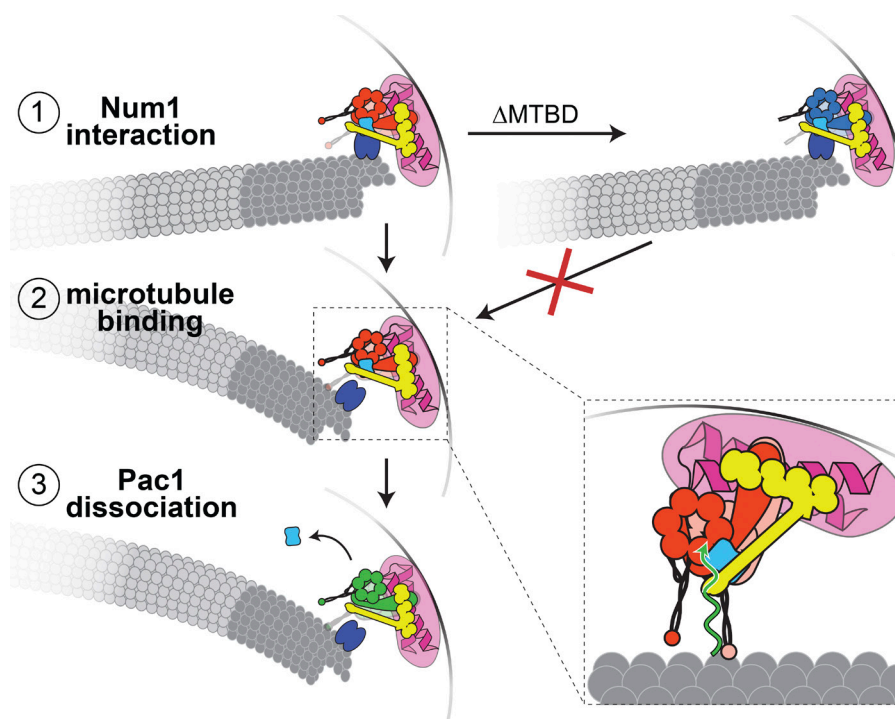
Figure 8. **Model for Num1-mediated activation of dynein-mediated spindle positioning.** Our data suggest that at the moment of offloading (step 1), contact between dynein–dynactin and cortical Num1 triggers a cascade of events that ultimately leads to Pac1 dissociation (step 3); however, the MTBD (deletion of which interrupts this process) is required to make contact with the microtubule to initiate Pac1 dissociation (step 2).

et al., 2003). Given the ability of Pac1 to reduce dynein motility in vitro (Markus and Lee, 2011; Huang et al., 2012), it has been postulated that Pac1 may hold dynein at plus ends in part by preventing its minus end–directed motility. At some point after or concomitant with dynein offloading, Pac1 dissociates from dynein and is never observed at cortical Num1 sites in wild-type cells (Lee et al., 2003). Given the observations presented here, we hypothesize that Num1 binding to dynein–dynactin triggers the dissociation of Pac1 from dynein. The fact that $Dyn1_{\Delta MTBD}$ is insensitive to $Num1_{CC}$ overexpression suggests that microtubule binding by dynein is a requisite for Pac1 dissociation. This suggests a mechanism whereby Num1 binding to the dynein tail domain (Markus et al., 2009) communicates allosteric changes to the motor head that, after microtubule binding, induce Pac1 dissociation from its binding site (at the junction between AAA3 and AAA4; Toropova et al., 2014) and consequently permit minus end–directed motility (see Fig. 8). The requisite microtubule binding by dynein for $Num1_{CC}$-mediated Pac1 dissociation likely explains the plus end colocalization of $Dyn1_{\Delta MTBD}$ with $Num1_{CC}$ (Fig. S5, A–C) and Pac1 (not depicted).

It is interesting to note the apparent discrepancies between the requirements for plus end binding of yeast and human dynein. In budding yeast, the dynein motor domain, Pac1, and Bik1 are absolutely essential (Lee et al., 2003; Sheeman et al., 2003; Markus et al., 2009), but dynactin is dispensable for this process (Lee et al., 2003). However, recent in vitro reconstitution experiments with human dynein revealed a distinct plus end binding complex that requires EB1, the p150Glued subunit of dynactin, and the full-length dynein complex (i.e., the motor domain is not sufficient; Duellberg et al., 2014). These latter observations, which did not describe any minus end–directed dynein motility, suggest that dynein and dynactin (or at least p150Glued) can interact at plus ends in the absence of the recently characterized adaptor proteins (e.g., Hook3, Spindly, and BicD2; McKenney et al., 2014; Schlager et al., 2014) and further suggest that their interaction is not sufficient for dynein motility.

Our observation that the MTBD of dynein is dispensable for plus end targeting was surprising and changes our understanding by which dynein recognizes and binds to microtubule plus ends. In light of this observation, we propose that dynein does not directly contact the plus end; rather, dynein associates with plus ends indirectly through its interactions with Pac1 and Bik1 (see Fig. 1 B). Evidence indicates that Pac1 enables dynein tip tracking in part by linking it to the plus end binding protein Bik1 (Sheeman et al., 2003; Roberts et al., 2014). Thus, the ability of Pac1 (and LIS1) to permit prolonged encounters between dynein and microtubules (McKenney et al., 2010; Huang et al., 2012) is likely unrelated to plus end binding by dynein in this organism. However, it is conceivable that by maintaining dynein in an off state at plus ends, Pac1 may prevent minus end motility of dynein motors that are in very close proximity to the microtubule. Upon binding of $Num1_{CC}$, dynein may pivot (likely in a stochastic manner) such that it may contact the plus end directly through its MTBD, subsequently release Pac1, and then walk toward the minus end. An analogous situation may take place in wild-type cells: after offloading to Num1 receptor sites at the cortex, dynein is well positioned to contact the microtubule to initiate spindle movements, which in turn may trigger Pac1 dissociation (Fig. 8). Recent structural studies support such a possibility: upon microtubule binding, conformational changes within the MTBD affect corresponding changes within the motor ring (Schmidt, 2015; Uchimura et al., 2015). These changes, which are propagated by the antiparallel coiled-coil that lead from the MTBD to the motor ring (via AAA4), could presumably affect Pac1 binding at the AAA3–AAA4 junction (see Fig. 8; Toropova et al., 2014).

Consistent with Num1 affecting the dynein-Pac1 interaction, the dynein mutant with higher than normal affinity for Pac1 ($Dyn1_{HL3}$) was much less susceptible to $Num1_{CC}$-mediated plus end depletion. It is unclear why $Dyn1_{HL3}$ exhibits higher affinity for Pac1. This mutant was engineered such that a helical linker was inserted between the tail and motor domains

(Markus and Lee, 2011). In the context of the tertiary structure of the dynein motor, this region lies in close proximity to the Pac1 binding site (between AAA3 and AAA4; see Fig. 5 A). Taken together with an apparent enhanced affinity of a tail-less dynein construct (motor domain only) for Pac1 (Reck-Peterson et al., 2006; Markus et al., 2009), it stands to reason that the tail domain plays a negative regulatory role in affecting Pac1 binding. Thus, whatever allosteric conformational change Num1$_{CC}$-dynein tail binding induces is likely interrupted by insertion of the helical HL3 linker.

The nature of the Num1$_{CC}$-dynein–dynactin interaction is currently unknown; however, a recent structural study revealed how human dynein–dynactin interacts with the coiled-coil–containing adaptor protein BicD2 (Urnavicius et al., 2015). Given the importance of the Num1 coiled-coil domain in the dynein–dynactin interaction, and the observation that Num1 (like BicD2) only interacts with intact dynein–dynactin complexes (Splinter et al., 2012), it may be that Num1 exhibits a similar mode of binding (i.e., direct contact with the dynein tail domain, and the Arp1 filament). Future high-resolution structural studies of the dynein tail domain within the context of the Num1$_{CC}$-dynein–dynactin complex will be necessary to understand the network of interactions that define this enormous protein complex, as well as how the tail domain may possibly affect Pac1-motor domain binding.

Materials and methods

Media and strain construction

All strains are derived from YEF473A (Bi and Pringle, 1996) and are listed in Table S1. We transformed yeast strains using the lithium acetate method (Knop et al., 1999). Strains carrying null mutations or fluorescently tagged components were constructed by PCR product-mediated transformation (Longtine et al., 1998) or by mating followed by tetrad dissection. Strains expressing mTurquoise2-Tub1 were generated as described (Markus et al., 2015). Transformants were clonally purified by streaking to individual colonies on selective media. Proper tagging was confirmed by PCR and, in some cases, sequencing. Yeast synthetic defined (SD) media were obtained from Sunrise Science Products.

To generate a yeast strain with point mutations in Num1$_{CC}$ (L167E L170E; Fig. 2 A), we used the site-specific genomic mutagenesis approach (Gray et al., 2004). In brief, after integration of the *URA3* cassette into the *num1$_{CC}$* locus (replacing nucleotides 499–510, corresponding to amino acids L167–L170), a PCR product amplified from pSM37 (see Plasmid construction) containing the desired nucleotide substitutions was transformed into the *URA3*-integrated strain and subsequently selected on 5-fluoroorotic acid–containing plates. 5-Fluoroorotic acid–resistant colonies were selected and confirmed by colony PCR and sequencing of the genomic DNA region. A similar method was used to delete the MTBD (residues 3,102–3,225) from *DYN1*.

To generate a yeast strain expressing the *GAL1p:PH-DYN1* allele, a cassette containing *KAN^R::GAL1p:PH* was amplified from pFA6a-kanMX6-pGAL1-PH (see Plasmid construction) and used for integration immediately upstream of the *DYN1-3mCherry* locus.

Plasmid construction

Using isothermal assembly (Gibson et al., 2009), we generated a plasmid in which the L167E L170E point mutations were engineered into a plasmid encoding Num1$_{CC(95–303)}$-PCN-S-TEV-ZZ (pBSG02; Tang et al.,

2012). In brief, primers were used to separately amplify the N-terminal (nucleotides 283–498, corresponding to amino acids 95–166) and C-terminal (nucleotides 511–909, corresponding to amino acids 171–303) portions of Num1$_{CC}$, such that the desired nucleotide substitutions were included in the reverse primer for the N-terminal portion and the forward primer for the C-terminal portion. After amplification, the 3′ and 5′ ends of the PCR products corresponding to the N- and C-terminal regions, respectively, contained 20 nucleotides of sequence identity with each other, whereas the 5′ and 3′ ends of the N- and C-terminal regions, respectively, contained 20 nucleotides of sequence identity with the NcoI- and NotI-digested pBSG02 vector. After digesting pBSG02 with NcoI and NotI (to excise Num1$_{CC(95–303)}$ wild type), the gel-purified PCR products and digested vector were assembled in vitro as described (Gibson et al., 2009). Proper assembly was verified by restriction digest and DNA sequencing and resulted in pSM37 (encoding Num1$_{CC(95–303)}^{LL/EE}$-PCN-S-TEV-ZZ).

To generate a plasmid with which to N-terminally tag Dyn1 with a PH domain, the PH domain of Num1 (amino acids 2,563–2,692) was amplified using a forward primer flanked with an XmaI site and a reverse primer flanked with a SalI site. The PCR product was digested with XmaI and SalI and ligated into pFA6a-kanMX6-PGAL1 (Longtine et al., 1998) digested similarly, yielding pFA6a-kanMX6-PGAL1-PH.

Image acquisition, analysis, and dynein motility assay

Yeast cultures were imaged after growth at 30°C to mid-log phase in synthetic defined media supplemented with either 2% glucose (SD plus glucose) or 2% galactose plus 2% raffinose (SD plus galactose/raffinose; the latter for induction of Num1$_{CC}$, Pac1, or Kip2, as indicated). To assess the effects of Num1$_{CC}$ on localization of dynein pathway components, *GAL1p:num1$_{CC}$* cells were induced in SD plus galactose/raffinose for 6 h before mounting cells for fluorescence microscopy. For wide-field fluorescence microscopy, yeast cells were imaged on an agarose pad containing 50 mM potassium phosphate buffer, pH 7, and images were collected at room temperature using a 1.49 NA 100× objective on a Ti-E inverted microscope equipped with a Ti-S-E motorized stage (Nikon), piezo Z-control (Physik Instrumente), a SOLA SM II LE LED light engine (Lumencor), a motorized filter cube turret, and an iXon X3 DU897 cooled EM-CCD camera (Andor). The microscope system was controlled by NIS-Elements software (Nikon). A step size of 1 µm was used to acquire 2-µm-thick Z-stack images. Sputtered/ET filter cube sets (Chroma Technology) were used for imaging mTurquoise2 (49001), GFP (49002), YFP (49003), and mCherry (49008) fluorescence.

Image analysis was performed using ImageJ software (National Institutes of Health; kymographs in Fig. 7 were generated with the MultipleKymograph plugin). Plus end and SPB foci were identified in two (or three) color movies and scored accordingly. Specifically, plus end molecules were recognized as those foci that localized to the distal tips of dynamic microtubules (identified via mTurquoise2-Tub1 imaging), whereas SPB molecules were recognized as those foci that localized to one of the spindle poles. Cortical molecules (e.g., in PH-Dyn1–expressing cells) were identified as those foci not associated with an astral microtubule plus end that remained stationary at the cell cortex for at least three frames. Two data sets were considered statistically significant if a Student's *t* test (assuming unequal variance) returned a p-value < 0.05.

For highly inclined and laminated optical sheet microscopy (Tokunaga et al., 2008), samples were prepared and imaged as above, except 488- and 561-nm lasers were used to excite YFP and mCherry, respectively. The laser illumination angle was adjusted individually for each sample to achieve the maximum signal-to-noise ratio. Emission filters were 525/50 nm for YFP and 600/50 for mCherry.

Purification of TAP (S tag-ZZ)-Dyn1-EGFP and the single-molecule motility assay (Fig. S1 and Video 1) were performed as previously described (Markus and Lee, 2011; Markus et al., 2012).

Cell lysis and immunoblotting

For Western blotting, yeast cultures were grown at 30°C in 3 ml of either SD plus glucose or SD plus galactose/raffinose and harvested. Equal numbers of cells were pelleted and resuspended in 0.2 ml of 0.1 M NaOH and incubated for 5 min at room temperature as described (Kushnirov, 2000). After centrifugation, the resulting cell pellet was resuspended in sample buffer and heated to ~100°C for 3 min. Lysates were separated on a 10% SDS polyacrylamide gel and electroblotted to PVDF in 25 mM Tris and 192 mM glycine supplemented with 0.05% SDS and 10% methanol for 30 min. Rabbit anti–c-Myc polyclonal (GenScript) or anti–α-tubulin (Applied Biological Materials, Inc.) monoclonal antibodies and HRP-conjugated goat anti–rabbit or anti–mouse antibody (Jackson ImmunoResearch Laboratories) were used at 1:1,000, 1:1,000, 1:3,000, or 1:3,000, respectively. The chemiluminescence signal was acquired on an ImageQuant LAS 500 gel documentation system. Immunoblots were exposed without saturating the camera's pixels.

Online supplemental material

Fig. S1 depicts the inherent ability of dynein to accumulate at microtubule minus ends in vitro. Fig. S2 shows that Num1$_{CC}$ overexpression depletes dynein light-intermediate (Dyn3) and intermediate (Pac11) chains, but not Bik1 from plus ends, and it also shows the effect of Num1$_{CC}$ overexpression on Dyn1 localization throughout the cell cycle. Fig. S3 shows the role of dynactin (Nip100), Pac1, and Bik1 in the Num1$_{CC}$-mediated plus end depletion phenotype. Fig. S4 shows additional examples of PH-dynein localization as well as its colocalization with dynactin (Jnm1). Fig. S5 shows the localization of Num1$_{CC}$-EGFP in various mutant backgrounds and also shows additional examples of the minus end–directed motility of Dyn1 in Num1$_{CC}$-overexpressing cells. Video 1 shows a representative in vitro dynein single-molecule assay. Video 2 shows plus end–directed molecules of dynein in Kip2- and Num1$_{CC}^{LL/EE}$-overexpressing cells, whereas Video 3 and Video 4 show minus end–directed molecules of dynein in Kip2- and Num1$_{CC}$-overexpressing cells. Table S1 shows strains used in this study. Online supplemental material is available at http://www.jcb.org/cgi/content/full/jcb.201506119/DC1.

References

Adames, N.R., and J.A. Cooper. 2000. Microtubule interactions with the cell cortex causing nuclear movements in *Saccharomyces cerevisiae*. *J. Cell Biol.* 149:863–874. http://dx.doi.org/10.1083/jcb.149.4.863

Ananthanarayanan, V., M. Schattat, S.K. Vogel, A. Krull, N. Pavin, and I.M. Tolić-Nørrelykke. 2013. Dynein motion switches from diffusive to directed upon cortical anchoring. *Cell.* 153:1526–1536. http://dx.doi.org/10.1016/j.cell.2013.05.020

Bi, E., and J.R. Pringle. 1996. ZDS1 and ZDS2, genes whose products may regulate Cdc42p in *Saccharomyces cerevisiae*. *Mol. Cell. Biol.* 16:5264–5275.

Carminati, J.L., and T. Stearns. 1997. Microtubules orient the mitotic spindle in yeast through dynein-dependent interactions with the cell cortex. *J. Cell Biol.* 138:629–641. http://dx.doi.org/10.1083/jcb.138.3.629

Carvalho, P., M.L. Gupta Jr., M.A. Hoyt, and D. Pellman. 2004. Cell cycle control of kinesin-mediated transport of Bik1 (CLIP-170) regulates microtubule stability and dynein activation. *Dev. Cell.* 6:815–829. http://dx.doi.org/10.1016/j.devcel.2004.05.001

Duellberg, C., M. Trokter, R. Jha, I. Sen, M.O. Steinmetz, and T. Surrey. 2014. Reconstitution of a hierarchical +TIP interaction network controlling microtubule end tracking of dynein. *Nat. Cell Biol.* 16:804–811. http://dx.doi.org/10.1038/ncb2999

Eshel, D., L.A. Urrestarazu, S. Vissers, J.C. Jauniaux, J.C. van Vliet-Reedijk, R.J. Planta, and I.R. Gibbons. 1993. Cytoplasmic dynein is required for normal nuclear segregation in yeast. *Proc. Natl. Acad. Sci. USA.* 90:11172–11176. http://dx.doi.org/10.1073/pnas.90.23.11172

Ferenz, N.P., R. Paul, C. Fagerstrom, A. Mogilner, and P. Wadsworth. 2009. Dynein antagonizes eg5 by crosslinking and sliding antiparallel microtubules. *Curr. Biol.* 19:1833–1838. http://dx.doi.org/10.1016/j.cub.2009.09.025

Gibson, D.G., L. Young, R.Y. Chuang, J.C. Venter, C.A. Hutchison III, and H.O. Smith. 2009. Enzymatic assembly of DNA molecules up to several hundred kilobases. *Nat. Methods.* 6:343–345. http://dx.doi.org/10.1038/nmeth.1318

Goshima, G., F. Nédélec, and R.D. Vale. 2005. Mechanisms for focusing mitotic spindle poles by minus end-directed motor proteins. *J. Cell Biol.* 171:229–240. http://dx.doi.org/10.1083/jcb.200505107

Gray, M., M. Kupiec, and S.M. Honigberg. 2004. Site-specific genomic (SSG) and random domain-localized (RDL) mutagenesis in yeast. *BMC Biotechnol.* 4:7. http://dx.doi.org/10.1186/1472-6750-4-7

Huang, J., A.J. Roberts, A.E. Leschziner, and S.L. Reck-Peterson. 2012. Lis1 acts as a "clutch" between the ATPase and microtubule-binding domains of the dynein motor. *Cell.* 150:975–986. http://dx.doi.org/10.1016/j.cell.2012.07.022

Kardon, J.R., S.L. Reck-Peterson, and R.D. Vale. 2009. Regulation of the processivity and intracellular localization of *Saccharomyces cerevisiae* dynein by dynactin. *Proc. Natl. Acad. Sci. USA.* 106:5669–5674. http://dx.doi.org/10.1073/pnas.0900976106

Knop, M., K. Siegers, G. Pereira, W. Zachariae, B. Winsor, K. Nasmyth, and E. Schiebel. 1999. Epitope tagging of yeast genes using a PCR-based strategy: more tags and improved practical routines. *Yeast.* 15(10B):963–972. http://dx.doi.org/10.1002/(SICI)1097-0061(199907)15:10B<963::AID-YEA399>3.0.CO;2-W

Kushnirov, V.V. 2000. Rapid and reliable protein extraction from yeast. *Yeast.* 16:857–860. http://dx.doi.org/10.1002/1097-0061(20000630)16:9<857::AID-YEA561>3.0.CO;2-B

Lee, W.L., J.R. Oberle, and J.A. Cooper. 2003. The role of the lissencephaly protein Pac1 during nuclear migration in budding yeast. *J. Cell Biol.* 160:355–364. http://dx.doi.org/10.1083/jcb.200209022

Lee, W.L., M.A. Kaiser, and J.A. Cooper. 2005. The offloading model for dynein function: differential function of motor subunits. *J. Cell Biol.* 168:201–207. http://dx.doi.org/10.1083/jcb.200407036

Li, Y.Y., E. Yeh, T. Hays, and K. Bloom. 1993. Disruption of mitotic spindle orientation in a yeast dynein mutant. *Proc. Natl. Acad. Sci. USA.* 90:10096–10100. http://dx.doi.org/10.1073/pnas.90.21.10096

Longtine, M.S., A. McKenzie III, D.J. Demarini, N.G. Shah, A. Wach, A. Brachat, P. Philippsen, and J.R. Pringle. 1998. Additional modules for versatile and economical PCR-based gene deletion and modification in Saccharomyces cerevisiae. *Yeast.* 14:953–961. http://dx.doi.org/10.1002/(SICI)1097-0061(199807)14:10<953::AID-YEA293>3.0.CO;2-U

Markus, S.M., and W.L. Lee. 2011. Regulated offloading of cytoplasmic dynein from microtubule plus ends to the cortex. *Dev. Cell.* 20:639–651. http://dx.doi.org/10.1016/j.devcel.2011.04.011

Markus, S.M., J.J. Punch, and W.L. Lee. 2009. Motor- and tail-dependent targeting of dynein to microtubule plus ends and the cell cortex. *Curr. Biol.* 19:196–205. http://dx.doi.org/10.1016/j.cub.2008.12.047

Markus, S.M., K.M. Plevock, B.J. St. Germain, J.J. Punch, C.W. Meaden, and W.L. Lee. 2011. Quantitative analysis of Pac1/LIS1-mediated dynein targeting: implications for regulation of dynein activity in budding yeast. *Cytoskeleton (Hoboken).* 68:157–174. http://dx.doi.org/10.1002/cm.20502

Markus, S.M., K.A. Kalutkiewicz, and W.L. Lee. 2012. She1-mediated inhibition of dynein motility along astral microtubules promotes polarized spindle movements. *Curr. Biol.* 22:2221–2230. http://dx.doi.org/10.1016/j.cub.2012.10.017

Markus, S.M., S. Omer, K. Baranowski, and W.L. Lee. 2015. Improved plasmids for fluorescent protein tagging of microtubules in *Saccharomyces cerevisiae*. *Traffic.* 16:773–786. http://dx.doi.org/10.1111/tra.12276

Matanis, T., A. Akhmanova, P. Wulf, E. Del Nery, T. Weide, T. Stepanova, N. Galjart, F. Grosveld, B. Goud, C.I. De Zeeuw, et al. 2002. Bicaudal-D regulates COPI-independent Golgi-ER transport by recruiting the dynein–dynactin motor complex. *Nat. Cell Biol.* 4:986–992. http://dx.doi.org/10.1038/ncb891

McKenney, R.J., M. Vershinin, A. Kunwar, R.B. Vallee, and S.P. Gross. 2010. LIS1 and NudE induce a persistent dynein force-producing state. *Cell.* 141:304–314. http://dx.doi.org/10.1016/j.cell.2010.02.035

McKenney, R.J., W. Huynh, M.E. Tanenbaum, G. Bhabha, and R.D. Vale. 2014. Activation of cytoplasmic dynein motility by dynactin-cargo adapter complexes. *Science.* 345:337–341. http://dx.doi.org/10.1126/science.1254198

Miura, M., A. Matsubara, T. Kobayashi, M. Edamatsu, and Y.Y. Toyoshima. 2010. Nucleotide-dependent behavior of single molecules of cytoplasmic dynein on microtubules in vitro. *FEBS Lett.* 584:2351–2355. http://dx.doi.org/10.1016/j.febslet.2010.04.016

Pease, J.C., and J.S. Tirnauer. 2011. Mitotic spindle misorientation in cancer—out of alignment and into the fire. *J. Cell Sci.* 124:1007–1016. http://dx.doi.org/10.1242/jcs.081406

Raaijmakers, J.A., M.E. Tanenbaum, and R.H. Medema. 2013. Systematic dissection of dynein regulators in mitosis. *J. Cell Biol.* 201:201–215. http://dx.doi.org/10.1083/jcb.201208098

Reck-Peterson, S.L., A. Yildiz, A.P. Carter, A. Gennerich, N. Zhang, and R.D. Vale. 2006. Single-molecule analysis of dynein processivity and stepping behavior. *Cell.* 126:335–348. http://dx.doi.org/10.1016/j.cell.2006.05.046

Roberts, A.J., B.S. Goodman, and S.L. Reck-Peterson. 2014. Reconstitution of dynein transport to the microtubule plus end by kinesin. *eLife.* 3:e02641. http://dx.doi.org/10.7554/eLife.02641

Rusan, N.M., U.S. Tulu, C. Fagerstrom, and P. Wadsworth. 2002. Reorganization of the microtubule array in prophase/prometaphase requires cytoplasmic dynein-dependent microtubule transport. *J. Cell Biol.* 158:997–1003. http://dx.doi.org/10.1083/jcb.200204109

Samora, C.P., B. Mogessie, L. Conway, J.L. Ross, A. Straube, and A.D. McAinsh. 2011. MAP4 and CLASP1 operate as a safety mechanism to maintain a stable spindle position in mitosis. *Nat. Cell Biol.* 13:1040–1050.

Schlager, M.A., H.T. Hoang, L. Urnavicius, S.L. Bullock, and A.P. Carter. 2014. In vitro reconstitution of a highly processive recombinant human dynein complex. *EMBO J.* 33:1855–1868. http://dx.doi.org/10.15252/embj.201488792

Schmidt, H. 2015. Dynein motors: how AAA+ ring opening and closing coordinates microtubule binding and linker movement. *BioEssays.* 37:532–543. http://dx.doi.org/10.1002/bies.201400215

Sheeman, B., P. Carvalho, I. Sagot, J. Geiser, D. Kho, M.A. Hoyt, and D. Pellman. 2003. Determinants of *S. cerevisiae* dynein localization and activation: implications for the mechanism of spindle positioning. *Curr. Biol.* 13:364–372. http://dx.doi.org/10.1016/S0960-9822(03)00013-7

Siller, K.H., and C.Q. Doe. 2009. Spindle orientation during asymmetric cell division. *Nat. Cell Biol.* 11:365–374. http://dx.doi.org/10.1038/ncb0409-365

Splinter, D., D.S. Razafsky, M.A. Schlager, A. Serra-Marques, I. Grigoriev, J. Demmers, N. Keijzer, K. Jiang, I. Poser, A.A. Hyman, et al. 2012. BICD2, dynactin, and LIS1 cooperate in regulating dynein recruitment to cellular structures. *Mol. Biol. Cell.* 23:4226–4241. http://dx.doi.org/10.1091/mbc.E12-03-0210

Tang, X., B.S. Germain, and W.L. Lee. 2012. A novel patch assembly domain in Num1 mediates dynein anchoring at the cortex during spindle positioning. *J. Cell Biol.* 196:743–756. http://dx.doi.org/10.1083/jcb.201112017

Tokunaga, M., N. Imamoto, and K. Sakata-Sogawa. 2008. Highly inclined thin illumination enables clear single-molecule imaging in cells. *Nat. Methods.* 5:159–161. http://dx.doi.org/10.1038/nmeth1171

Toropova, K., S. Zou, A.J. Roberts, W.B. Redwine, B.S. Goodman, S.L. Reck-Peterson, and A.E. Leschziner. 2014. Lis1 regulates dynein by sterically blocking its mechanochemical cycle. *eLife.* 3:3. http://dx.doi.org/10.7554/eLife.03372

Uchimura, S., T. Fujii, H. Takazaki, R. Ayukawa, Y. Nishikawa, I. Minoura, Y. Hachikubo, G. Kurisu, K. Sutoh, T. Kon, et al. 2015. A flipped ion pair at the dynein-microtubule interface is critical for dynein motility and ATPase activation. *J. Cell Biol.* 208:211–222. http://dx.doi.org/10.1083/jcb.201407039

Urnavicius, L., K. Zhang, A.G. Diamant, C. Motz, M.A. Schlager, M. Yu, N.A. Patel, C.V. Robinson, and A.P. Carter. 2015. The structure of the dynactin complex and its interaction with dynein. *Science.* 347:1441–1446. http://dx.doi.org/10.1126/science.aaa4080

Williams, S.E., S. Beronja, H.A. Pasolli, and E. Fuchs. 2011. Asymmetric cell divisions promote Notch-dependent epidermal differentiation. *Nature.* 470:353–358. http://dx.doi.org/10.1038/nature09793

Woodruff, J.B., D.G. Drubin, and G. Barnes. 2009. Dynein-driven mitotic spindle positioning restricted to anaphase by She1p inhibition of dynactin recruitment. *Mol. Biol. Cell.* 20:3003–3011. http://dx.doi.org/10.1091/mbc.E09-03-0186

Yamada, M., S. Toba, Y. Yoshida, K. Haratani, D. Mori, Y. Yano, Y. Mimori-Kiyosue, T. Nakamura, K. Itoh, S. Fushiki, et al. 2008. LIS1 and NDEL1 coordinate the plus-end-directed transport of cytoplasmic dynein. *EMBO J.* 27:2471–2483. http://dx.doi.org/10.1038/emboj.2008.182

Yang, Z., U.S. Tulu, P. Wadsworth, and C.L. Rieder. 2007. Kinetochore dynein is required for chromosome motion and congression independent of the spindle checkpoint. *Curr. Biol.* 17:973–980. http://dx.doi.org/10.1016/j.cub.2007.04.056
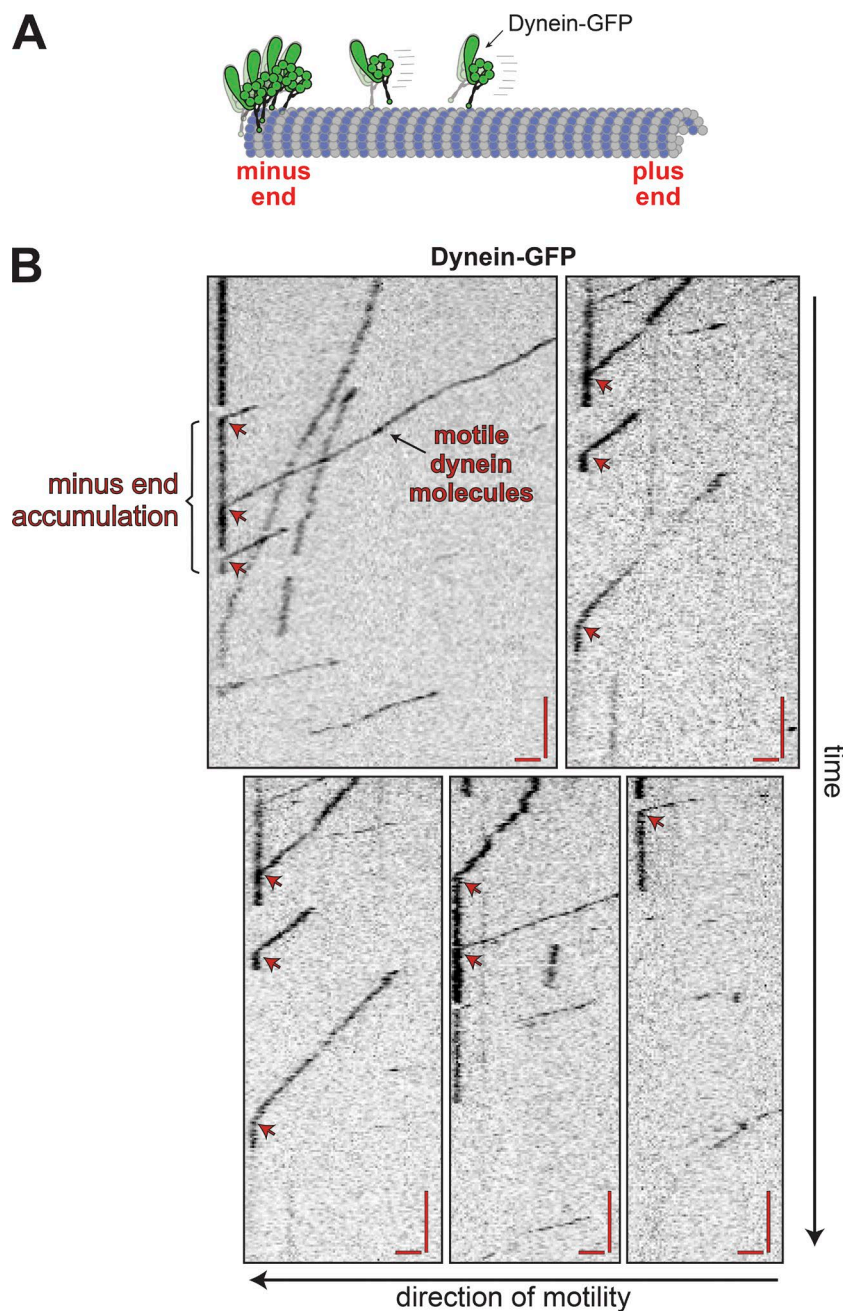
THE JOURNAL OF CELL BIOLOGY

Figure S1. **Purified dynein motors pause at microtubule minus ends before detaching.** Schematic (A) and example kymographs (B) depicting single molecules of purified dynein motors walking toward and then pausing at the minus end of a taxol-stabilized microtubule before detaching. The dwell time of ~0.1 s per step was approximated based on a mean velocity of 85 nm/s and a mean center-of-mass step size of 8 nm (Reck-Peterson et al., 2006). Bars: (vertical) 1 min; (horizontal) 2 µm. Also see Video 1. Related to Fig. 1.
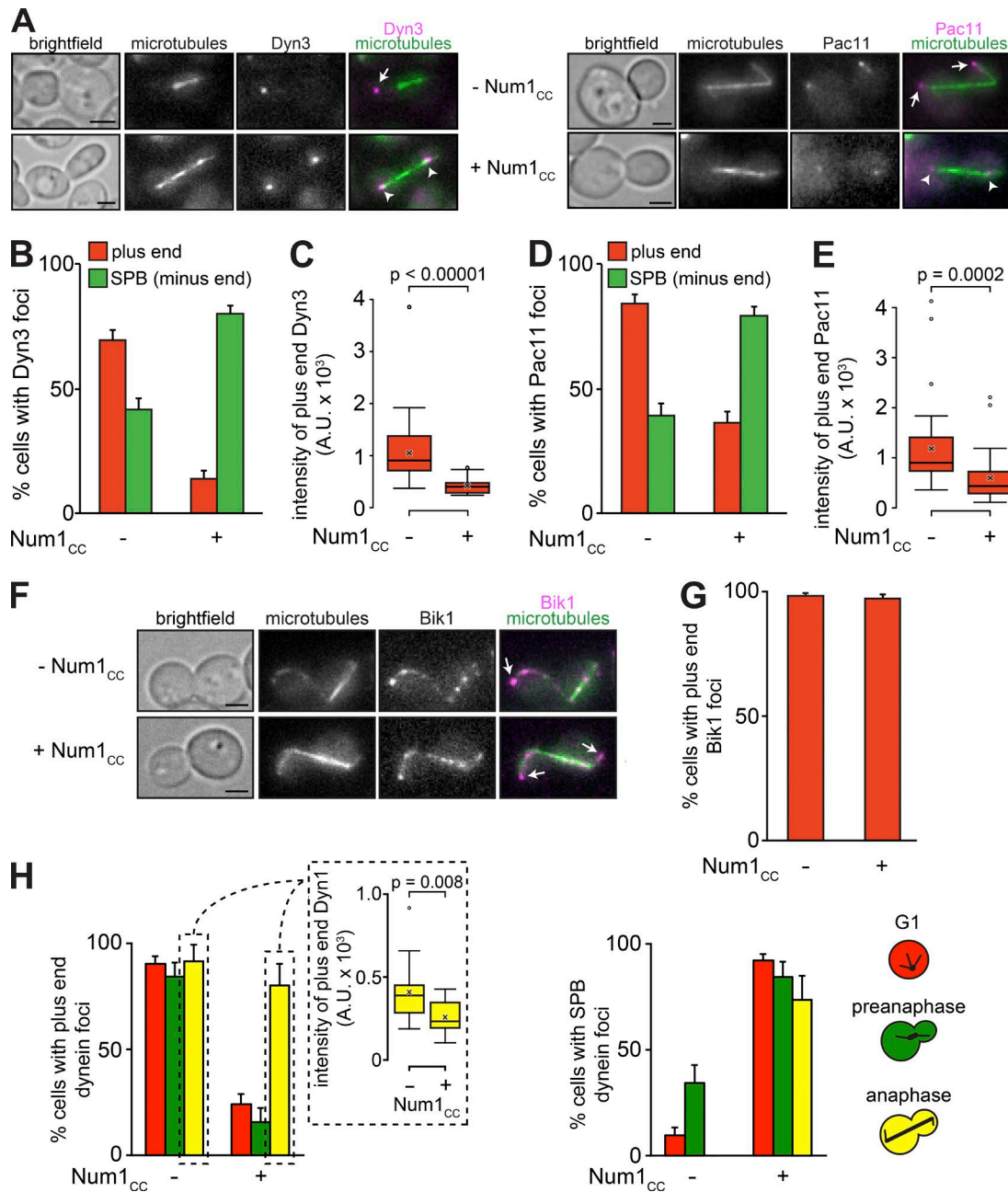
Figure S2. **Overexpression of Num1$_{CC}$ depletes dynein light-intermediate and intermediate chains, but not Bik1 from microtubule plus ends, and assessment of Num1$_{CC}$-affected dynein localization throughout the cell cycle.** (A) Representative images of *GAL1p:num1$_{CC}$* cells expressing mTurquoise2-Tub1 and either Dyn3- (left) or Pac11-3mCherry (right) used for quantitation in B–E. Cells were cultured as described in Fig. 1. (B–E) Frequency (B and D) and plus end intensity (C and E) of Dyn3- (left) and Pac11-3mCherry (right) in uninduced cells or cells induced to overexpress Num1$_{CC}$. Plus end or SPB foci were identified in two-color movies and scored accordingly. In B and D, error bars represent the standard error of proportion ($n \geq 102$ cells). For box plots in C and E ($n \geq 19$ foci), whiskers define the range of data, boxes encompass the 25th to 75th quartiles, the line depicts the median value, and the "x" depicts the mean value. (F) Representative images of *GAL1p:num1$_{CC}$* cells expressing mTurquoise2-Tub1 and Bik1-3mCherry used for quantitation in G. (G) The percentage of cells that exhibit plus end Bik1-3mCherry foci is plotted. Error bars represent the standard error of proportion ($n \geq 115$ cells). (H) The percentage of cells in the indicated phase of the cell cycle that exhibit plus end (left) or SPB (right) localized Dyn1-3mCherry foci in uninduced cells or cells induced to express Num1$_{CC}$ ($n \geq 63$, 32, or 12 cells for G1, preanaphase, or anaphase, respectively). The inset shows fluorescence intensity measurements for Dyn1-3mCherry at the plus ends of anaphase spindle microtubules ($n \geq 16$ foci). All images are maximum-intensity projections of a 2-µm Z-stack of wide-field images. Arrows indicate plus end foci, and arrowheads indicate SPB foci. Bars, 2 µm. Related to Fig. 1.
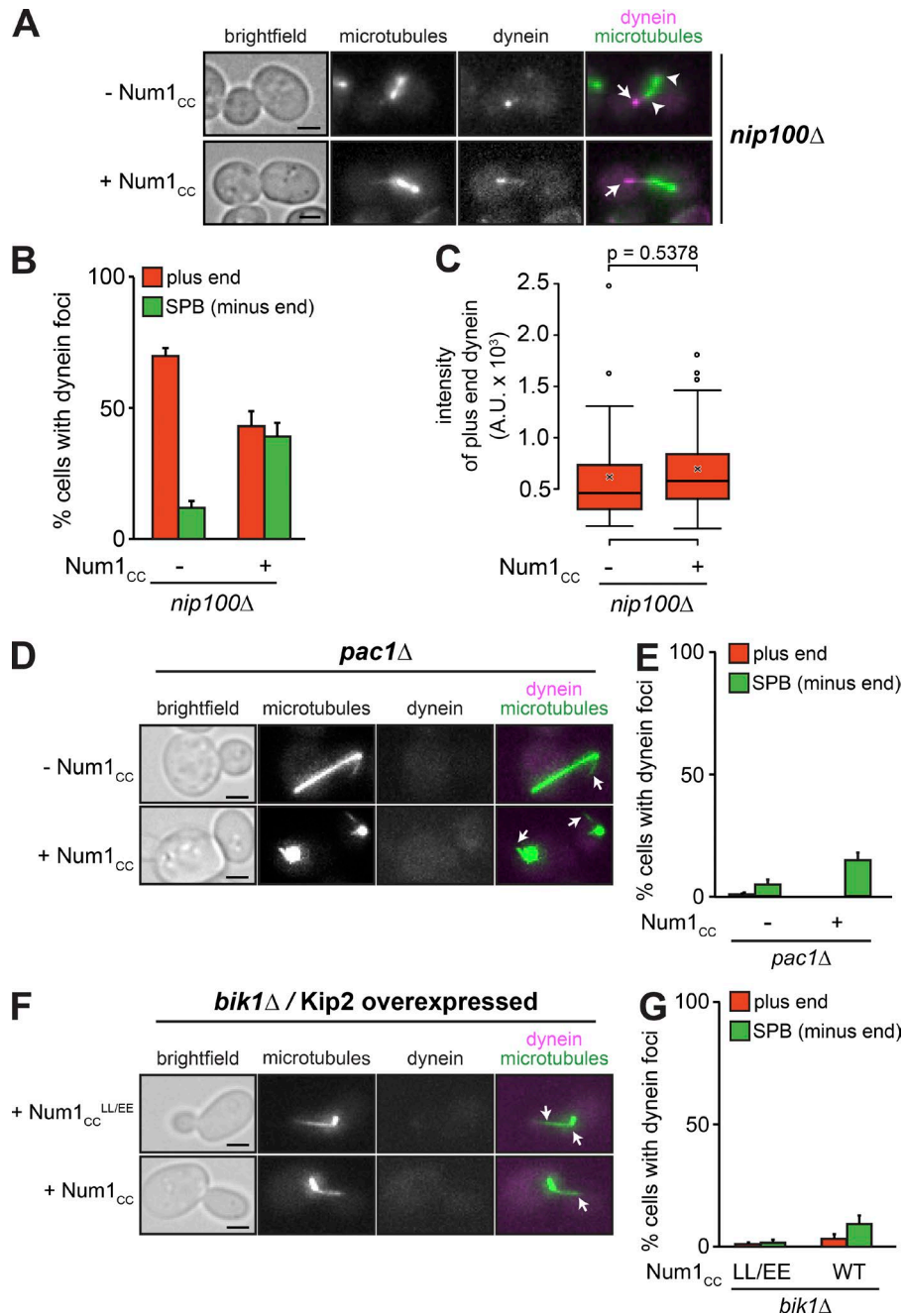
Figure S3. **Complete Num1$_{CC}$-mediated depletion of dynein from plus ends requires dynactin, and plus end targeting is a requisite for robust SPB localization of dynein in Num1$_{CC}$-overexpressing cells.** (A) Representative images of *GAL1p:num1$_{CC}$ nip100Δ* cells expressing mTurquoise2-Tub1 and Dyn1-3mCherry used for quantitation in B. (B) The percentage of cells that exhibit plus end (red) or SPB (green) Dyn1-3mCherry foci is plotted for the cells shown in A. Error bars represent the standard error of proportion (*n* ≥ 169 cells). (C) Box plot of fluorescence intensity values of plus end–associated Dyn1-3mCherry (*n* ≥ 30 foci). Whiskers define the range of data, boxes encompass the 25th to 75th quartiles, the line depicts the median value, and the "x" depicts the mean value. Related to Fig. 1. (D) Representative images of *GAL1p:num1$_{CC}$ pac1Δ* cells cultured in either SD plus glucose or SD plus galactose/raffinose used for quantitation in E. (E) The percentage of cells that exhibit plus end (red) or SPB (green) Dyn1-3mCherry foci is plotted for the cells shown in D. Error bars represent the standard error of proportion (*n* ≥ 111 cells). (F) Representative images illustrating Dyn1-3mCherry targeting in *bik1Δ* cells overexpressing Num1$_{CC}$ or Num1$_{CC}$$^{LL/EE}$. To compensate for the short astral microtubule phenotype in *bik1Δ* cells (Berlin et al., 1990), we overexpressed Kip2 using the *GAL1p:KIP2* allele, which, when induced, restores microtubule lengths to near wild-type (WT) levels. For this reason, we compared *GAL1p:num1$_{CC}$ GAL1p:KIP2 bik1Δ* (bottom) with *GAL1p:num1$_{CC}$$^{LL/EE}$ GAL1p:KIP2 bik1Δ* cells (top), both of which were cultured in SD plus galactose/raffinose (to induce overexpression of Kip2 and either Num1$_{CC}$ or Num1$_{CC}$$^{LL/EE}$). (G) The percentage of cells that exhibit plus end (red) or SPB (green) Dyn1-3mCherry foci is plotted for the cells shown in F. Error bars represent the standard error of proportion (*n* ≥ 64 cells). All images are maximum-intensity projections of a 2-μm Z-stack of wide-field images. For A, arrows indicate plus end foci, and arrowheads indicate SPB foci. For D and F, arrows indicate plus ends without foci. Bars, 2 μm. Related to Fig. 1.
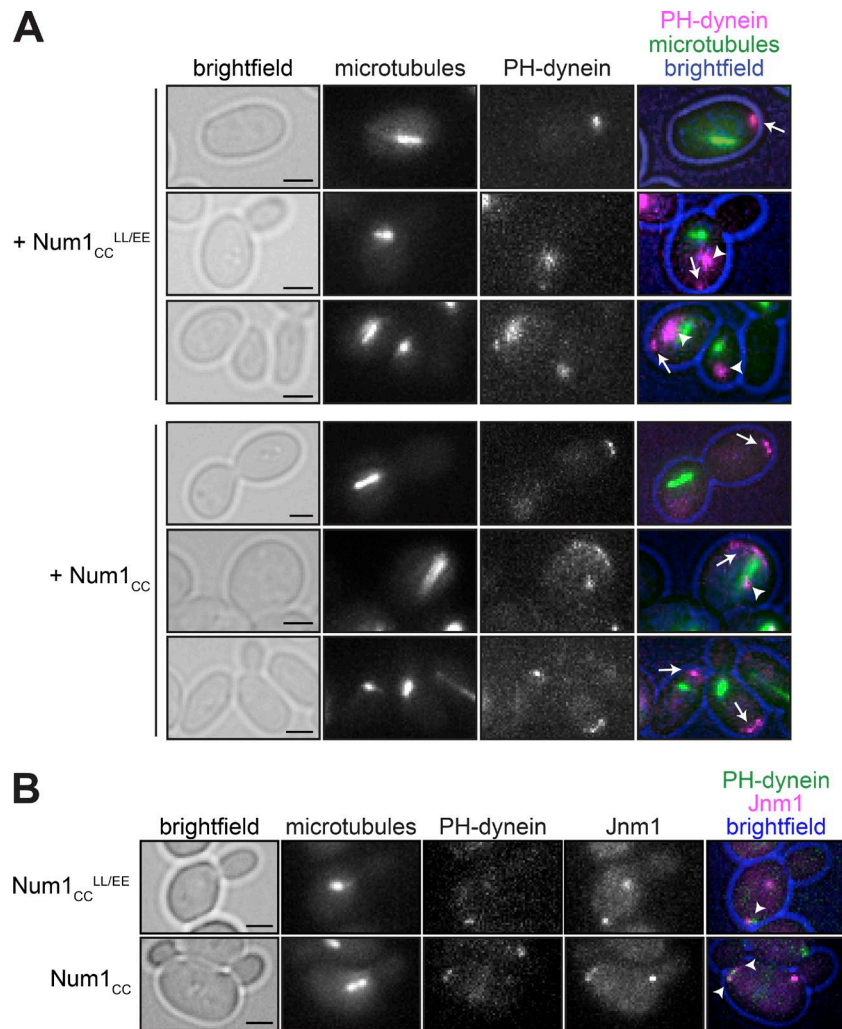
Figure S4.   **Num1$_{CC}$ overexpression affects the size of PH-Dyn1-3mCherry cortical patches, and cortical PH-Dyn1 foci colocalize with dynactin.** (A) Representative images of cells induced to express PH-Dyn1-3mCherry and either Num1$_{CC}$$^{LL/EE}$ (top) or Num1$_{CC}$ (bottom). Cells were grown as described in Fig. 1. Arrows indicate cortical dynein patches; arrowheads indicate motile cytoplasmic foci not associated with microtubule-based structures (presumably aggregates). (B) Representative images of *GAL1p:PH-DYN1-3mCherry* cells expressing Jnm1-3YFP and either Num1$_{CC}$ or Num1$_{CC}$$^{LL/EE}$ (as indicated). Arrowheads indicate colocalized cortical PH-Dyn1-Jnm1 foci. All images are maximum-intensity projections of a 2-µm Z-stack of wide-field images. Bars, 2 µm. Related to Fig. 4.
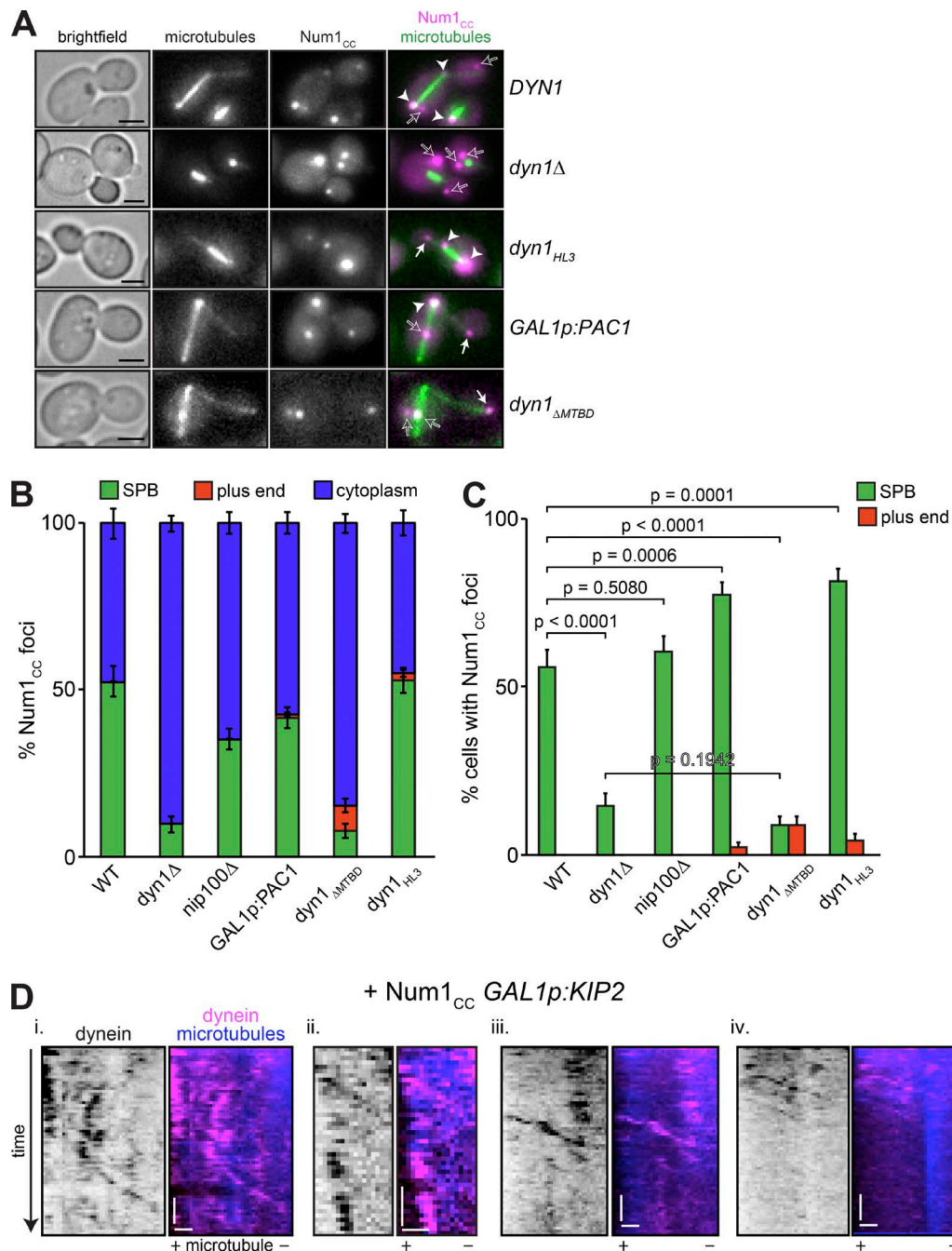
Figure S5.   **Localization of Num1$_{CC}$ mirrors that of dynein, and additional examples of Num1$_{CC}$-induced minus end–directed dynein motility.** (A) Representative images of cells induced to express Num1$_{CC}$-EGFP with the indicated genotype used for quantitation in B and C. Cells were grown as described in Fig. 1. Each image is a maximum-intensity projection of a 2-µm Z-stack of wide-field images. Open arrows indicate cytoplasmic foci, closed arrows indicate plus end foci, and arrowheads indicate SPB foci. Bars, 2 µm. Plus end, SPB, or cytoplasmic foci were identified in two-color movies and scored accordingly. (B) The percentage of Num1$_{CC}$-EGFP foci that localize to the SPB (green), plus end (red), or cytoplasm (blue) is plotted ($n \geq 116$ foci). (C) The percentage of cells that exhibit plus end (red) or SPB (green) Num1$_{CC}$-EGFP foci is plotted for the cells shown in A. Error bars in B and C represent the standard error of proportion ($n \geq 89$ cells). Given the lack of colocalization between Num1$_{CC}$ and microtubules, these data also suggest that Num1$_{CC}$ is not sufficient to bind microtubules. (D) Additional example kymographs depicting minus end–directed motility of dynein along astral microtubules in cells overexpressing Num1$_{CC}$ and Kip2. Kymographs were generated from time-lapse images acquired using highly inclined and laminated optical sheet microscopy (see Materials and methods). Bars: (vertical) 1 min; (horizontal) 1 µm. Related to Figs. 3, 5, 6, and 7. WT, wild type.
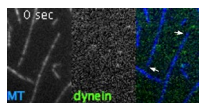

Video 1.   **In vitro motility of single Dyn1-EGFP molecules purified from yeast cells.** Time-lapse total internal reflection fluorescence microscope images of single Dyn1-EGFP molecules (green in merge) walking along taxol-stabilized microtubules (blue in merge) and pausing at the minus ends (arrows). Also see Fig. S1. Related to Fig. 1.
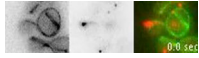
Video 2.   **Plus end–directed motility of dynein molecules in Kip2- and Num1$_{CC}^{LL/EE}$-overexpressing cells.** Time-lapse highly inclined and laminated optical sheet images of Dyn1-3mCherry molecules (inverse fluorescence image in middle panel; red in merge) walking along astral microtubules (inverse fluorescence image in left panel; green in merge) toward the plus ends. Note the long astral microtubule phenotype is attributable to Kip2 overexpression. Related to Fig. 7.
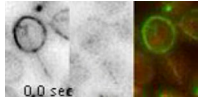
Video 3.   **Minus end–directed motility of dynein molecules in Kip2- and Num1$_{CC}$-overexpressing cells.** Time-lapse highly inclined and laminated optical sheet images of Dyn1-3mCherry molecules (inverse fluorescence image in middle panel; red in merge) walking along astral microtubules (inverse fluorescence image in left panel; green in merge) toward the minus ends. Related to Fig. 7.
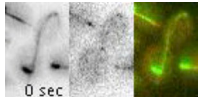
Video 4.   **Minus end–directed motility of dynein molecules in Kip2- and Num1$_{CC}$-overexpressing cells.** Time-lapse highly inclined and laminated optical sheet images of Dyn1-3mCherry molecules (inverse fluorescence image in middle panel; red in merge) walking along astral microtubules (inverse fluorescence image in left panel; green in merge) toward the minus ends. Related to Fig. 7.

Table S1. **Strains used in this study**

Strain	Genotype	Source
SMY4	*Mata ura3-52 lys2-801 leu2-Δ1 his3-Δ200 trp1-Δ63*	Vorvis et al., 2008
SMY165	*Matα KAN^R::GAL1p-TAP-Dyn1-EGFP::TRP1 ura3-52 trp1 lys2-801 leu2Δ1 his3Δ200 pep4::HIS3 prb1Δ1.6R can1 GAL*	Markus and Lee, 2011
SMY357	*Mata TRP1::GAL1p:num1$_{CC}$::KAN^R Dyn1-3mCherry::HIS3 TUB1::HPH::HIS3p:mTurquoise2-Tub1 ura3-52 lys2-801 leu2-Δ1 his3-Δ200 trp1-Δ63*	This study
SMY358	*Matα TRP1::GAL1p:num1$_{CC}$::KAN^R Dyn1-3mCherry::HIS3 nip100Δ::KANR TUB1::HPH::HIS3p:mTurquoise2-Tub1 ura3-52 lys2-801 leu2-Δ1 his3-Δ200 trp1-Δ63*	This study
SMY373	*Mata TRP1::GAL1p:num1$_{CC}$::KAN^R Jnm1-3mCherry::HIS3 TUB1::HPH::HIS3p:mTurquoise2-Tub1 ura3-52 lys2-801 leu2-Δ1 his3-Δ200 trp1-Δ63*	This study
SMY385	*Mata TRP1::GAL1p:num1$_{CC}^{LL/EE}$::KAN^R Dyn1-3mCherry::HIS3 TUB1::HPH::HIS3p:mTurquoise2-Tub1 ura3-52 lys2-801 leu2-Δ1 his3-Δ200 trp1-Δ63*	This study
SMY390	*Mata TRP1::GAL1p:num1$_{CC}$::KAN^R Dyn1$_{HL3}$-3YFP::TRP1 TUB1::HPH::HIS3p:mTurquoise2-Tub1 ura3-52 lys2-801 leu2-Δ1 his3-Δ200 trp1-Δ63*	This study
SMY398	*Mata TRP1::GAL1p:num1$_{CC}$::KAN^R Dyn1-3YFP::TRP1 Pac1-3mCherry::HIS3 TUB1::HPH::HIS3p:mTurquoise2-Tub1 ura3-52 lys2-801 leu2-Δ1 his3-Δ200 trp1-Δ63*	This study
SMY392	*Mata TRP1::GAL1p:num1$_{CC}$-13myc::KAN^R ura3-52 lys2-801 leu2-Δ1 his3-Δ200 trp1-Δ63*	This study
SMY399	*TRP1::GAL1p:num1$_{CC}$::KAN^R Dyn1-3mCherry::HIS3 KAN^R::GAL1p:PAC1 TUB1::HPH::HIS3p:mTurquoise2-Tub1 ura3-52 lys2-801 leu2-Δ1 his3-Δ200 trp1-Δ63*	This study
SMY402	*Matα TRP1::GAL1p:num1$_{CC}$::KAN^R dyn1Δ::Dyn1$_{MOTOR}$-3YFP::TRP1 TUB1::HPH::HIS3p:mTurquoise2-Tub1 ura3-52 lys2-801 leu2-Δ1 his3-Δ200 trp1-Δ63*	This study
SMY406	*Mata TRP1::GAL1p:num1$_{CC}$::KAN^R Pac1-3mCherry::HIS3 Dyn1$_{HL3}$::TRP1 TUB1::HPH::HIS3p:mTurquoise2-Tub1 ura3-52 lys2-801 leu2-Δ1 his3-Δ200 trp1-Δ63*	This study
SMY408	*Mata TRP1::GAL1p:num1$_{CC}$::KAN^R Bik1-3mCherry::HIS3 Dyn1-3YFP::TRP1 GFP-TUB1::LEU2 ura3-52 lys2-801 leu2-Δ1 his3-Δ200 trp1-Δ63*	This study
SMY415	*Matα TRP1::GAL1p:num1$_{CC}$::KAN^R Dyn3-3mCherry::HIS Dyn1-3YFP::TRP TUB1::HPH::HIS3p:mTurquoise2-Tub1 ura3-52 lys2-801 leu2-Δ1 his3-Δ200 trp1-Δ63*	This study
SMY440	*Mata TRP1::GAL1p:num1$_{CC}$::KAN^R KAN^R::GAL1p:KIP2 Dyn1-3mCherry::HIS3 TUB1::HPH::HIS3p:mTurquoise2-Tub1 ura3-52 lys2-801 leu2-Δ1 his3-Δ200 trp1-Δ63*	This study
SMY457	*Matα TRP1::GAL1p:num1$_{CC}$::KAN^R dyn1$_{ΔMTBD}$-3mCherry::HIS3 TUB1::HPH::HIS3p:mTurquoise2-Tub1 ura3-52 lys2-801 leu2-Δ1 his3-Δ200 trp1-Δ63*	This study
SMY469	*Mata TRP1::GAL1p:num1$_{CC}$-EGFP::LEU2 nip100Δ::KAN^R TUB1::HPH::HIS3p:mRuby2-Tub1 ura3-52 lys2-801 leu2-Δ1 his3-Δ200 trp1-Δ63*	This study
SMY470	*Mata TRP1::GAL1p:num1$_{CC}$-EGFP::LEU2 dyn1$_{HL3}$::TRP1 TUB1::HPH::HIS3p:mRuby2-Tub1 ura3-52 lys2-801 leu2-Δ1 his3-Δ200 trp1-Δ63*	This study
SMY472	*Matα TRP1::GAL1p:num1$_{CC}$-EGFP::LEU2 dyn1Δ::HIS3 TUB1::HPH::HIS3p:mRuby2-Tub1 ura3-52 lys2-801 leu2-Δ1 his3-Δ200 trp1-Δ63*	This study
SMY474	*Mata TRP1::GAL1p:num1$_{CC}$-EGFP::LEU2 TUB1::HPH::HIS3p:mRuby2-Tub1 ura3-52 lys2-801 leu2-Δ1 his3-Δ200 trp1-Δ63*	This study
SMY475	*Mata TRP1::GAL1p:num1$_{CC}$-EGFP::LEU2 Dyn1-3mCherry::HIS3 KAN^R::GAL1p:PAC1 TUB1::HPH::HIS3p:mRuby2-Tub1 ura3-52 lys2-801 leu2-Δ1 his3-Δ200 trp1-Δ63*	This study
SMY479	*Matα TRP1::GAL1p:num1$_{CC}^{LL/EE}$::KAN^R KAN^R::GAL1p:KIP2 Dyn1-3mCherry::HIS3 TUB1::HPH::HIS3p:mTurquoise2-Tub1 ura3-52 lys2-801 leu2-Δ1 his3-Δ200 trp1-Δ63*	This study
SMY485	*Mata TRP1::GAL1p:num1$_{CC}$::KAN^R Pac11-3mCherry::HIS3 TUB1::HPH::HIS3p:mTurquoise2-Tub1 ura3-52 lys2-801 leu2-Δ1 his3-Δ200 trp1-Δ63*	This study
SMY497	*Mata TRP1::GAL1p:num1$_{CC}^{LL/EE}$-13myc::KAN^R ura3-52 lys2-801 leu2-Δ1 his3-Δ200 trp1-Δ63*	This study
SMY503	*Matα TRP1::GAL1p:num1$_{CC}$-EGFP::LEU2 dyn1$_{ΔMTBD}$-3mCherry::HIS3 TUB1::HPH::HIS3p:mTurquoise2-Tub1 ura3-52 lys2-801 leu2-Δ1 his3-Δ200 trp1-Δ63*	This study
SMY530	*Matα TRP1::GAL1p:num1$_{CC}$::KAN^R Dyn1-3mCherry::HIS pac1Δ::HIS3 TUB1::HPH::HIS3p:mTurquoise2-Tub1 ura3-52 lys2-801 leu2-Δ1 his3-Δ200 trp1-Δ63*	This study
SMY608	*Matα TRP1::GAL1p:num1$_{CC}$::KAN^R KAN^R::GAL1p:PH-Dyn1-3mCherry::HIS3 Jnm1-3YFP::LEU2 TUB1::HPH::HIS3p:mTurquoise2-Tub1 ura3-52 lys2-801 leu2-Δ1 his3-Δ200 trp1-Δ63*	This study
SMY609	*Matα TRP1::GAL1p:num1$_{CC}^{LL/EE}$::KAN^R KAN^R::GAL1p:PH-Dyn1-3mCherry::HIS3 Pac1-3YFP::LEU2 TUB1::HPH::HIS3p:mTurquoise2-Tub1 ura3-52 lys2-801 leu2-Δ1 his3-Δ200 trp1-Δ63*	This study
SMY610	*Matα TRP1::GAL1p:num1$_{CC}^{LL/EE}$::KAN^R KAN^R::GAL1p:PH-Dyn1-3mCherry::HIS3 Jnm1-3YFP::LEU2 TUB1::HPH::HIS3p:mTurquoise2-Tub1 ura3-52 lys2-801 leu2-Δ1 his3-Δ200 trp1-Δ63*	This study
SMY618	*Mat a KAN^R::GAL1p:PAC1 TRP1::GAL1p:num1$_{CC}^{LL/EE}$::KAN^R Dyn1-3mCherry::HIS3 TUB1::HPH::HIS3p:mTurquoise2-Tub1 ura3-52 lys2-801 leu2-Δ1 his3-Δ200 trp1-Δ63*	This study
SMY633	*Matα TRP1::GAL1p:num1$_{CC}$::KAN^R KAN^R::GAL1p:KIP2 Dyn1-3mCherry::HIS3 Spc110-Venus::LEU2 TUB1::HPH::HIS3p:mTurquoise2-Tub1 ura3-52 lys2-801 leu2-Δ1 his3-Δ200 trp1-Δ63*	This study
SMY635	*Matα TRP1::GAL1p:num1$_{CC}^{LL/EE}$::KAN^R KAN^R::GAL1p:KIP2 Dyn1-3mCherry::HIS3 Spc110-Venus::LEU2 TUB1::HPH::HIS3p:mTurquoise2-Tub1 ura3-52 lys2-801 leu2-Δ1 his3-Δ200 trp1-Δ63*	This study
SMY639	*Matα TRP1::GAL1p:num1$_{CC}$::KAN^R KAN^R::GAL1p:KIP2 bik1Δ::HIS3 Dyn1-3mCherry::HIS3 TUB1::HPH::HIS3p:mTurquoise2-Tub1 ura3-52 lys2-801 leu2-Δ1 his3-Δ200 trp1-Δ63*	This study
SMY640	*Matα TRP1::GAL1p:num1$_{CC}^{LL/EE}$::KAN^R KAN^R::GAL1p:KIP2 bik1Δ::HIS3 Dyn1-3mCherry::HIS3 TUB1::HPH::HIS3p:mTurquoise2-Tub1 ura3-52 lys2-801 leu2-Δ1 his3-Δ200 trp1-Δ63*	This study

Table S1. **Strains used in this study** *(Continued)*

Strain	Genotype	Source
SMY696	*Matα TRP1::GAL1p:num1$_{CC}$::KAN^R Jnm1-3mCherry::HIS3 dyn1$_{ΔMTBD}$ TUB1::URA3::HIS3p:mTurquoise2-Tub1 ura3-52 lys2-801 leu2-Δ1 his3-Δ200 trp1-Δ63*	This study
SMY713	*Matα TRP1::GAL1p:num1$_{CC}$::KAN^R Nip100-3mCherry::HIS3 dyn1$_{ΔMTBD}$ TUB1::HPH::HIS3p:mTurquoise2-Tub1 ura3-52 lys2-801 leu2-Δ1 his3-Δ200 trp1-Δ63*	This study
SMY814	*Matα TRP1::GAL1p:num1$_{CC}$::KAN^R GST-dyn1$_{motor}$-3mCherry::HIS3 TUB1::HPH::HIS3p:mTurquoise2-Tub1 ura3-52 lys2-801 leu2-Δ1 his3-Δ200 trp1-Δ63*	This study
SMY855	*Matα TRP1::GAL1p:num1$_{CC}$::KAN^R KAN^R::GAL1p:PH-Dyn1-3mCherry::HIS3 Pac1-3YFP::LEU2 TUB1::HPH::HIS3p:mTurquoise2-Tub1 ura3-52 lys2-801 leu2-Δ1 his3-Δ200 trp1-Δ63*	This study

References

Berlin, V., C.A. Styles, and G.R. Fink. 1990. BIK1, a protein required for microtubule function during mating and mitosis in *Saccharomyces cerevisiae*, colocalizes with tubulin. *J. Cell Biol.* 111:2573–2586. http://dx.doi.org/10.1083/jcb.111.6.2573

Markus, S.M., and W.L. Lee. 2011. Regulated offloading of cytoplasmic dynein from microtubule plus ends to the cortex. *Dev. Cell.* 20:639–651. http://dx.doi.org/10.1016/j.devcel.2011.04.011

Reck-Peterson, S.L., A. Yildiz, A.P. Carter, A. Gennerich, N. Zhang, and R.D. Vale. 2006. Single-molecule analysis of dynein processivity and stepping behavior. *Cell.* 126:335–348. http://dx.doi.org/10.1016/j.cell.2006.05.046

Vorvis, C., S.M. Markus, and W.L. Lee. 2008. Photoactivatable GFP tagging cassettes for protein-tracking studies in the budding yeast *Saccharomyces cerevisiae*. *Yeast.* 25:651–659. http://dx.doi.org/10.1002/yea.1611